

OMEGA: A Low-Latency GNN Serving System for Large Graphs

Geon-Woo Kim[§], Donghyun Kim[§], Jeongyoon Moon[§], Henry Liu[§], Tarannum Khan[§],
Anand Iyer[†], Daehyeok Kim[§], Aditya Akella[§]

[§]The University of Texas at Austin

[†]Georgia Institute of Technology

Abstract

Graph Neural Networks (GNNs) have been widely adopted for their ability to compute expressive node representations in graph datasets. However, serving GNNs on large graphs is challenging due to the high communication, computation, and memory overheads of constructing and executing computation graphs, which represent information flow across large neighborhoods. Existing approximation techniques in training can mitigate the overheads but, in serving, still lead to high latency and/or accuracy loss. To this end, we propose OMEGA, a system that enables low-latency GNN serving for large graphs with minimal accuracy loss through two key ideas. First, OMEGA employs *selective recomputation of pre-computed embeddings*, which allows for reusing precomputed computation subgraphs while selectively recomputing a small fraction to minimize accuracy loss. Second, we develop *computation graph parallelism*, which reduces communication overhead by parallelizing the creation and execution of computation graphs across machines. Our evaluation with large graph datasets and GNN models shows that OMEGA significantly outperforms state-of-the-art techniques.

1 Introduction

Graph Neural Networks (GNNs) have gained widespread attention due to their ability to provide breakthrough results in diverse domains [30, 33, 35, 70, 83, 99]; they have been instrumental in discovering life-saving drugs [59, 69], empowered recommendation systems [68, 89], and helped in traffic planning [14, 27, 47]. Recent studies have enabled reasoning on graph-structured data [11, 67, 74, 87, 94] by enhancing large language models (LLMs) [12, 18, 40, 81] with GNNs to effectively capture intricate structural information.

The GNN lifecycle consists of two phases: *training* and *serving*. In the training phase [15, 31, 34, 57, 61, 78, 96], GNNs take as input graph-structured data and feature vectors of each node (Fig. 1 (left)), and learn the *embeddings* of each node in the graph. In the serving phase [41, 56, 72, 89, 91], the trained model is used to predict the embeddings for previously unseen *query* nodes. Such predictions empower downstream GNN use-cases, such as malicious node prediction in financial applications and social media [13, 27, 48], and integration with LLMs [23, 82].

Ensuring low latency in computing the embeddings of query nodes is key to GNN serving, as GNN models are increasingly used in time-sensitive tasks, including recommendation [56, 76, 89], fraud detection [8, 60], and traffic prediction [28]. At the same time, the underlying graphs are growing in size; modern industry graph datasets routinely span a few billion nodes and trillions of edges [58] and can consume hundreds of TB of memory. Distributing such large graph datasets and associated feature vectors across multiple machines is thus inevitable these days.

Unfortunately, achieving low-latency GNN serving for large graphs stored across machines is extremely challenging. To compute the embeddings of the query nodes, GNN models need the entire k -hop neighborhood. The number of k -hop neighbors can grow exponentially with k , known as the neighborhood explosion problem [19, 37, 90]. Serving query nodes can thus require excessive amounts of memory and computation costs due to the size of feature vectors and adjacency matrix in the large neighborhood.

Furthermore, unlike training, we do not know how an incoming query node will be connected to the rest of the graph; no matter how the large graph is partitioned and stored, the k -hop neighbors of a query node and their feature vectors are often spread across multiple machines. As a result, creating the query node's "computation graph" (Fig. 1 (right)), by which the node's embedding is computed based on the neighborhood's feature vectors and aggregation paths along the edges, involves fetching the associated data from remote partitions; the resulting massive data volumes (§3.1) cause high communication overheads, worsening serving latency.

GNN training systems facing similar issues adopt mitigation techniques based on *approximation*, such as reusing historical embeddings [32, 65] or sampling [34, 57, 58, 78]. However, we find they are not directly applicable to serving for two reasons: (a) they do not account for the *data dependence* between an incoming query node and the existing graph – i.e., determining how the query node's connectivity impacts the embeddings of the graph's existing nodes. Ignoring such dependence can lead to unacceptably high accuracy loss (§3.2). (b) While existing techniques reduce computation (either by reusing node embeddings or computing embeddings for fewer nodes by sampling), we find that the communication involved

is still heavy at inference time because of the underlying graph’s rich connectivity and the query node’s neighborhood being spread across machines.

We present OMEGA, a GNN serving system that combines data dependency-aware approximation with a new form of computation parallelism to systematically address the overheads, supporting low-latency GNN serving on modern large graphs with minimal accuracy loss. Existing serving systems either adopt sampling [56, 72, 89] (with concomitant high latency or substantial accuracy loss) or apply to smaller graphs [41, 91], limiting their practical applicability (§9).

Similar to some training systems [32, 65], OMEGA reuses embeddings of existing nodes after training (which we call "precomputed embeddings (PEs)") instead of computing the embeddings in the entire k -hop neighborhood; this saves network, compute, and memory resources. Because naïvely reusing PEs ignores data dependence and undermines accuracy, OMEGA uses *Selective Recomputation of Precomputed Embeddings* (SRPE) (§5). Here, we identify a small number of neighborhood nodes that impact accuracy substantially and focus on recomputing their embeddings while reusing PEs for other nodes. We prove that this statistically minimizes approximation errors. We develop a practical heuristic to perform recomputation on such nodes within a budget, where the budget trades off latency with accuracy.

SRPE significantly reduces the size of computation graphs, but it still entails substantial communication (§8.3) due to fetching remote PEs and feature vectors. To mitigate this overhead, we develop *Computation Graph Parallelism* (CGP) (§6). Unlike existing GNN systems where a single machine solely creates computation graphs by fetching required data from remote machines, CGP allows each machine to build a partitioned computation graph using data available in local partitions. CGP then aggregates the partitioned computations using efficient all-to-all collectives and finally applies *custom merge functions* (tailored to the specific type of GNN model) to the aggregations to compute the final outputs.

We implement OMEGA based on DGL [78, 96], a popular GNN training framework, and evaluate it on representative graph datasets and GNN models. Our evaluation results show that the combination of SRPE and CGP helps OMEGA outperform DGL-based full-graph and approximation-drive baseline serving systems by up to $159\times$ and $10.8\times$ in latency, respectively, with minimal accuracy loss (§8).

We make the following contributions in this paper:

- We show that naïvely applying approximation techniques and reusing computations leads to large errors, and propose SRPE, which statistically minimizes these errors by identifying the parts of computation graphs that need recomputation to avoid accuracy losses (§5).
- We co-design CGP, a new parallelism technique that reduces communication overheads of SRPE with local aggregation by parallelizing the creation and execution of computation graphs for serving various GNN models (§6).

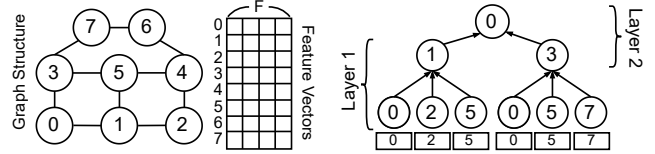


Figure 1: (Left) An example graph dataset with 8 nodes and F -dimensional feature vectors. We use this graph dataset as our running example. (Right) The 2-hop computation graph for node 0 where the boxes below represent feature vectors.

- We show that OMEGA is able to outperform state-of-the-art techniques and to achieve up to orders of magnitude lower latency with minimal accuracy loss (§8).

2 Background

A Primer on GNNs. Unlike conventional deep neural networks (DNNs) that process independent input vectors without considering their inter-dependencies, GNNs are designed to handle graph datasets. These datasets consist of node feature vectors and a graph structure that expresses the relationships between nodes, as depicted in Fig. 1 (left). For instance, in social networks, users are the nodes, their profiles are the feature vectors, and friendships are the edges.

GNN models aggregate the neighborhood information of each node to leverage the relationships and compute highly expressive *embeddings* than individual feature vectors alone. To achieve this, the first step is to create a *computation graph* that contains the k -hop neighborhood of each node along with the associated feature vectors, where k is typically 2 or more [38]. A GNN model then *executes* the computation graph to iteratively generate the embedding of a target node. Starting with the feature vectors of the farthest k -hop neighbors, the GNN model applies DNN operations and an aggregation function at each hop, where each step represents a layer in the GNN model until the embedding for the target node is computed. Fig. 1 (right) illustrates an example of a 2-hop computation graph for a node.

The computation of GNN models typically leverages *message passing* [36, 78], which we can generally express as follows. For a target node v and layer $1 \leq l \leq k$, define:

$$h_v^{(l)} = U^{(l)}(h_v^{(l-1)}, \bigoplus_{u \in N(v)} \{M^{(l)}(h_u^{(l-1)})\}) \quad (1)$$

where $h_u^{(0)}$ is the feature vector for node u , $N(v)$ represents direct neighbors of the node v , and $h_v^{(k)}$ is the final embedding for the node v . Each GNN layer defines (U, \bigoplus, M) functions, which represent *update*, *aggregate*, and *message* function, respectively. The message function is applied to the neighbors of node v to create *messages*, which are aggregated by the aggregate function. The layer embedding of each layer is then obtained by applying the update function to the previous layer embedding of node v and the aggregated messages.

GNN Serving for Large Graphs. Similar to conventional DNN models, GNN models can be trained on a static graph

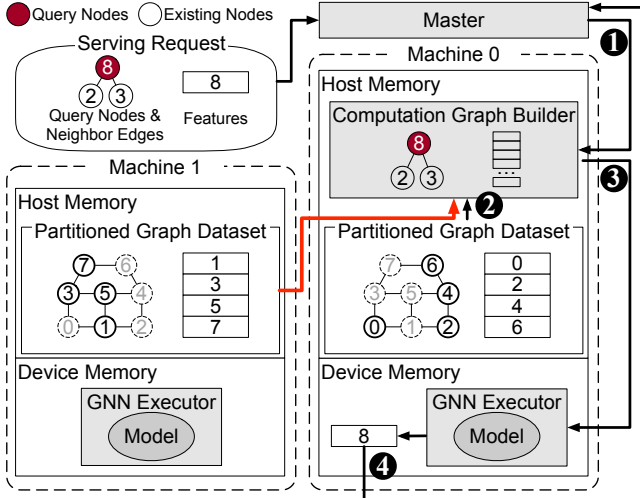


Figure 2: Distributed GNN serving end-to-end workflow. To generate the embeddings of (batched) query nodes, ① the master forwards a serving request to one machine. ② A computation graph builder then creates k -hop computation graphs for the query nodes by loading from the local partition and fetching required edges and feature vectors from remote partitions. The red line represents remote communication. ③ The computation graphs are then executed by a GNN executor after being copied into GPU device memory. ④ Finally, the embeddings of the query nodes are returned.

dataset in the background. However, unlike DNN serving, which only needs a trained model, GNN serving additionally requires the graph dataset used in training because of the data dependency in GNN computation. To serve a large graph dataset (e.g., 2 billion nodes and 2 trillion edges [58]), the dataset needs to be distributed across multiple machines [34, 58, 86, 97], and the embeddings for the new *query* nodes are computed with this distributed data.

Fig. 2 illustrates a workflow of distributed GNN serving systems. Here, a training graph dataset is partitioned across multiple machines. A *serving request* consists of the feature vectors of query nodes and the edges between the query nodes and the existing training nodes. When one of the machines receives the request, it creates computation graphs by fetching the required feature vectors and edges from the other machines, computes the embeddings of the query nodes, and returns the result.

3 Challenges

Unfortunately, the size of graph datasets that distributed GNN serving systems can handle is limited due to unique properties of modern graph data, especially, the data dependency between query nodes and existing graph nodes, which leads to high overheads. Existing mitigation techniques often fall well short due to fundamental drawbacks.

Method	Latency (ms)	Accuracy (%)
Full Computation Graph (Full)	711.1	56.9
Neighborhood Sampling (NS)	168.8	50.9 (-6.0)
Historical Embeddings (HE)	66.4	50.6 (-6.3)

Table 1: Latency and accuracy of different serving methods. We run serving requests of batch size 1,024 with 4 machines. A 3-Layer Graph Attention Networks [75] trained on the Yelp dataset [90] is used. We describe the detailed setup in §8.1.

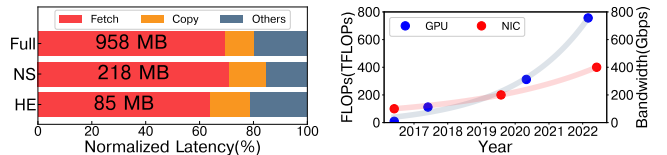


Figure 3: (Left) Latency breakdown of Table 1. The data size in each bar indicates the amount of feature vectors and edges fetched. (Right) Trendlines of peak FP32 FLOPs of NVIDIA GPUs [1, 5–7] and bandwidth of NVIDIA NICs [2–4].

3.1 Overheads from Large Neighborhoods

GNN serving requires the entire k -hop neighborhood in computing the embeddings of query nodes. Since the number of k -hop neighbors can grow exponentially with k , memory and compute costs can be also significant to create and execute computation graphs, which contain the feature vectors and edges corresponding to the neighborhood. For example, serving with the full (neighborhood) computation graph in Table 1 can take 711 ms, likely violating the tight latency SLOs of real-world applications [66, 93, 98]. Here, the computation overhead is substantial, as shown in blue in Fig. 3. Also, the memory overhead from these large neighborhoods can easily lead to GPU out-of-memory errors despite their tens of GB memory capacity (§8.2).

Moreover, it is hard to predict how query nodes are connected to the rest of the graph and as such feature vectors and edges can be stored across multiple machines (as shown in Fig. 2); thus, creating computation graphs involves fetching neighborhood information and the corresponding feature vectors from remote partitions (Step ②), resulting in high communication overhead, shown in red in Fig. 3.

3.2 Limitations of Today’s Approximations

To mitigate problems due to large neighborhoods and overheads, one could employ approximation taking inspiration from similar techniques in GNN *training* systems. Unfortunately, this can lead to significant model accuracy loss (Table 1) and, in some cases, may not improve latency.

Historical Embeddings. Instead of creating full computation graphs every iteration, GNN training systems [32, 65] reuse the layer embeddings from previous iterations, called *historical embeddings* [20, 32]. This technique avoids the exponential expansion of computation graphs, allowing GNN training systems to construct computation graphs only with direct neighbors. Since model parameters are updated at each

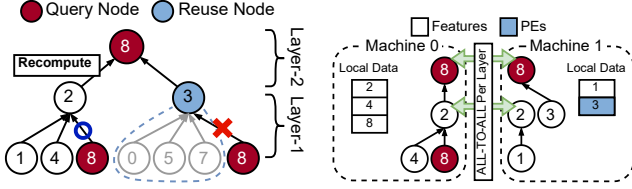


Figure 4: High-level illustration of (Left) Selective Recomputation of Precomputed Embeddings (SRPE) and (Right) Computation Graph Parallelism (CGP). The query node 8 is connected to the existing nodes 2 and 3 of the example graph dataset in Fig. 1.

iteration, historical embeddings introduce approximation errors. Over multiple training epochs, the training systems address the errors using an auxiliary loss function or updating historical embeddings based on their staleness [32, 65]. One may consider applying this technique to serving by reusing the layer embeddings from the last training epoch. However, as the embeddings are data dependency-unaware, i.e., they do not account for how new query nodes impact existing embeddings, using them for serving can hurt accuracy. As shown in Table 1, although serving can be 10.7 \times faster with this technique, it results in a 6.3% points drop in accuracy.

Sampling. GNN training systems [31, 34, 57, 58, 71, 78, 86, 88, 92, 96] employ *sampling* with which they aggregate only a small number of sampled neighbors at each hop [19, 22, 37, 90]. This drastically reduces the size of the computation graph at the cost of accuracy due to approximation errors from sampling. Multiple training epochs are executed to account for the accuracy loss, and each epoch samples the computation graph differently. Running many epochs leads to convergence. However, in serving, we find that a sampled computation graph can hurt accuracy significantly (6.0% points drop in Table 1) since we do not have multiple chances to recover approximation errors from sampling. Moreover, latency can be still high because, even with sampling, the size of computation graphs and the associated communication overhead can be significant (§8.2).

Furthermore, even with either approximation, over 80% of the latency is still spent fetching the associated feature vectors (Fig. 3), where feature dimensions typically range from hundreds to thousands [42, 89, 92], from remote partitions and copying them into the GPU memory. We observe that the communication overhead is a key bottleneck in GNN serving for large graphs regardless of GNN models and graph datasets (§8.3). Recent trends in GPU and NIC performance (Fig. 3 (right)) further indicate that communication will remain a challenge in large-scale GNN serving.

4 OMEGA Overview

Our system, OMEGA, addresses GNN serving challenges and overheads due to large neighborhoods through two complementary techniques: smart data dependency-aware approximation and distributed computation graph creation/execution.

T-1: Selective Recomputation of Precomputed Embeddings (§5).

To deal with neighborhood explosion, we design a technique called selective recomputation of precomputed embeddings (SRPE) that reduces redundant computations of layer embeddings by effectively reusing previously computed embeddings named *precomputed embeddings* (PE). Unlike historical embeddings used in training (§3.2), SRPE mitigates accuracy drops by *selectively recomputing* a portion of the PEs that contributes to high approximation errors. SRPE decides on recomputation nodes based on a simple but effective heuristic policy that statistically minimizes the approximation errors. Fig. 4 (left) illustrates an example usage of SRPE. After training, SRPE precomputes the embedding of existing training nodes. When computing the embedding of query node 8, SRPE reuses the PE of node 3 while *recomputing* the PE of node 2 to better reflect the contribution of node 8 (i.e., the edge from node 8 to 2 at Layer-1).

T-2: Computation Graph Parallelism and Custom Merge Functions (§6).

While SRPE reduces the size of computation graphs and corresponding computational overheads, it still has high communication overhead due to fetching PEs and feature vectors; e.g., we find that SRPE alone can still yield latencies as high as 978 ms (§8.3) due to the overhead. To further minimize this overhead, we develop *computation graph parallelism* (CGP), which distributes both *creation* and *execution* of computation graphs across multiple machines. In CGP, each machine carefully constructs a *partitioned computation graph* to use only local feature vectors and PEs during execution, thus avoiding heavy remote communication. For instance, in Fig. 4 (right), to compute the Layer-1 embedding of node 2, Machine 0 uses local feature vectors of nodes 4 and 8, while Machine 1 uses the local feature vector of node 1. However, since each machine has a partial view of the entire neighborhood, conventional message passing computation (Eq. 1) fails to generate correct outputs. To overcome this challenge, CGP employs a form of distributed execution that extends message passing with collective communications and *custom merge functions* tailored to various GNN models.

End-to-end Workflow.

Fig. 5 illustrates the end-to-end workflow of OMEGA. The PEs of all nodes in the training graph dataset are computed after training and distributed across machines along with the graph dataset. ① Upon the arrival of a serving request containing a batch of query nodes, the master server evenly splits the query nodes, their feature vectors, and the neighbor edges. ② The partitioned requests are then distributed to the computation graph builder in each machine, ③ which creates a partitioned computation graph. When building the computation graph, each builder determines which PEs to *recompute* and adds the edges required for the recomputation to the computation graph. ④ Copied to GPU memory, the partitioned computation graphs are executed by GNN executors, which employ local aggregations followed by collective communications to generate the final output embeddings with

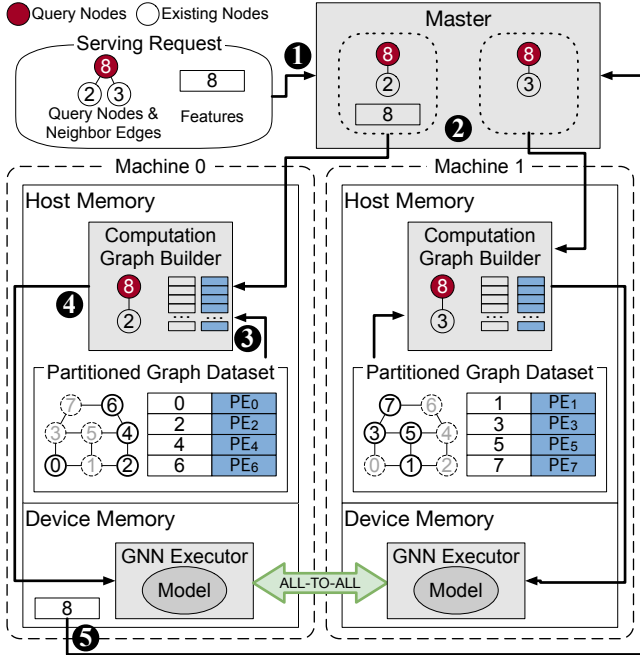


Figure 5: OMEGA end-to-end workflow.

customized merge functions for GNN models; 5 the master server collects and returns the output embeddings.

Problem Scope. This paper focuses on achieving low-latency, large-scale GNN serving for *new* query nodes that are unseen during training, while mitigating large computational overheads and approximation errors (§3). We assume that GNN models are trained on a fixed graph (e.g., the example graph dataset in Fig. 1), and during the serving phase, query nodes arrive with edges connecting them to training nodes in the fixed graph (e.g., query node 8 in Fig. 5 is connected to nodes 2 and 3). Addressing potential staleness problems and enabling dynamic updates of graph datasets, GNN models, and PEs is left for future work.

5 Selective Recomputation of PE

To mitigate the overheads from large neighborhoods (§3), OMEGA reuses precomputed embeddings (PEs), $p_u^{(l)}$ for each node u and layer l ($1 \leq l \leq k-1$), which are captured from the layer embeddings (i.e., $h_u^{(l)}$ in Eq. 1) after training. During the serving phase, for a query node v , OMEGA computes the final embedding $h_v^{(k)}$ without fully recalculating the embeddings for the full k -hop neighborhood. Instead, it substitutes the embeddings of v 's direct neighbors with their respective PEs, utilizing $p_u^{(l)}$ in place of computing $h_u^{(l)}$. This approach significantly reduces both computational complexity and memory requirements from $O(N^k)$ to $O(N \times k)$, where N represents the average number of neighbors.

5.1 Skewed Approximation Errors of PEs

However, we observe that naively reusing PEs for GNN serving can lead to substantial reductions in model accuracy, such as 6.3% points decrease (denoted HE in Table 1). This re-

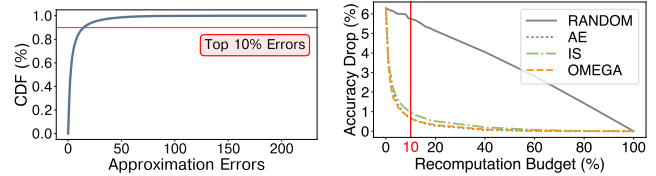


Figure 6: (Left) CDF of the approximation errors of PEs, derived from the workload in Table 1. We randomly selected 25% of test nodes as query nodes, computed PEs with the remaining nodes, and aggregated the errors using the query nodes. (Right) Effectiveness of various recomputation policies in restoring accuracy with increasing recomputation budgets. ‘AE’ and ‘IS’ represent recomputation based on actual approximation errors and node importance scores. ‘OMEGA’ denotes the proposed query edge ratio-based policy (§5.2.2).

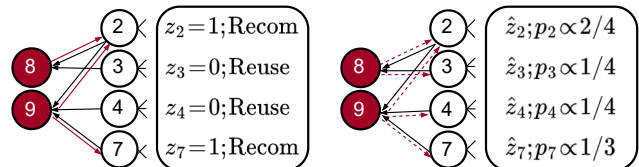


Figure 7: An example of selective recomputation in a batch of two query nodes: 8 (connected to nodes 2 and 3) and 9 (connected to nodes 2, 4, and 7). (Left) Recomputation of two candidates given a 50% recomputation budget. (Right) Random variables with recomputation probabilities such that $\sum p_i = 0.5$. OMEGA’s policy assigns each probability proportional to the ratio of edges from the query nodes.

duction is attributed to approximation errors in PEs. These errors occur because PEs are snapshotted after training, failing to aggregate the embeddings from new query nodes. For example, the PE of node 3 shown in Fig. 4 (left) is computed considering only the neighbors in the training graph (nodes 0, 5, 7), excluding the new query node 8.

We quantify the approximation errors by computing the difference between the *full embeddings*, $f_u^{(l)}$, which include all the edges from query nodes in aggregation, and the PEs. When u is a direct neighbor of query nodes, we compute its PE approximation error as $\sum_{l=1}^{k-1} \|f_u^{(l)} - p_u^{(l)}\|$.

We observe that the approximation errors are *highly skewed* – the errors from a small number of PEs mainly contribute to accuracy losses. Fig. 6 (left) shows a distribution of the approximation errors of PEs. The top 10% of PE approximation errors are several orders larger than the other 90%. More importantly, recomputing the 10% of PEs, while reusing the other PEs, effectively recovers accuracy drop from -6.3% points to -0.7% points (AE in Fig. 6 (right)). Exploiting the skew in approximation errors is key to the effectiveness of recomputation; e.g., randomly selecting the 10% recomputation targets (RANDOM in Fig. 6 (right)) yields a marginal accuracy benefit (from -6.3% points to -5.7% points).

5.2 Policy for Selective PE Recomputation

Based on the observation, we propose to *selectively* recompute PEs that show high approximation errors when used to serve query nodes. The key challenge in this approach lies in devising an effective *recomputation policy* that can identify PEs prone to high approximation errors.

5.2.1 Problem Formulation

We describe the problem of selective PE recomputation and the objective of recomputation policies, using an example of serving two query nodes (i.e., nodes 8 and 9) in Fig. 7 (left). In this example, we can utilize PEs of the direct neighbors of the query nodes (i.e., nodes 2, 3, 4, and 7), which we call *recomputation candidates*. A policy decides whether to recompute or reuse the PE for each candidate node. Recomputation includes the edges from query nodes to a candidate node, whereas reuse ignores them. Then, the objective of the recomputation policy is to find the best recomputation targets, given a recomputation budget, that minimizes the approximation errors of the candidates. Fig. 7 (left) illustrates an example where the budget allows for two out of four PEs to be recomputed.

The recomputation policy can be formulated as a constrained optimization problem as follows:

$$\min_{z \in \{0,1\}^{|R|}} \sum_{u \in R} \sum_{l=1}^{k-1} \|f_u^{(l)} - h_{G_z, u}^{(l)}\| \quad \text{sub. to.} \quad \sum_{u \in R} z_u \leq \gamma |R| \quad (2)$$

Here, R is the recomputation candidates, z is a $|R|$ -sized 0-1 vector deciding recomputation of each candidate, G_z denotes the corresponding graph, $h_{G_z, u}$ represents the approximated embeddings in G_z , and f_u are the full embeddings. Finally, γ refers to the budget.

However, directly solving the problem at serving time is challenging because it is impractical to compute the full embeddings. Instead, we stochastically approximate the constrained optimization problem. As illustrated in Fig. 7 (right), we assign independent binary random variables \hat{z}_u to each candidate u such that it has a recomputation probability of $p_u = \mathbb{E}[\hat{z}_u]$, within the budget $\gamma = \sum_u p_u$.

In this setting, our goal is to find the optimal probabilities that minimize the approximation errors. To achieve this, we adopt the variance minimization technique from recent work in sampling-based GNN training [90]; we define unbiased estimators for the full embeddings and derive the optimal recomputation probabilities that minimize the variance of the estimators. By selecting candidates with high probabilities, we can indirectly reduce the approximation errors.

We develop unbiased estimators for the full embeddings. For each u , the full embedding $f_u^{(l)}$ is computed with aggregations from the query nodes ($q_u^{(l)}$) and those from the training nodes ($t_u^{(l)}$). Here, we simplify the aggregation as the mean of the messages from neighbors; for example, $q_u^{(l)} = \sum_{v \in N_Q(u)} m_v^{(l)} / |N(u)|$ where $N_Q(u)$ denotes the query

nodes connected to u and $m_v^{(l)}$ are the messages. Then, we define the estimator $\hat{f}_u^{(l)} = \frac{1}{p_u} \hat{z}_u q_u^{(l)} + t_u^{(l)}$ such that $\mathbb{E}[\hat{f}_u^{(l)}] = f_u^{(l)}$. We obtain the optimal probabilities that minimize the variance of the estimators with the following theorem.

Theorem 1 *The sum of the variances of every dimension of the estimators ($\sum_u \sum_{l=1}^{k-1} \hat{f}_u^{(l)}$) is minimized when $p_u \propto \|\sum_{l=1}^{k-1} q_u^{(l)}\| = \|\sum_{l=1}^{k-1} \sum_{v \in N_Q(u)} \frac{m_v^{(l)}}{|N(u)}\|$, given $\gamma = \sum_u p_u$.*

The proof is based on *Theorem 3.2.* from [90]. With the constant sum of probabilities γ , we can derive the lower bound of the estimator using the Cauchy-Schwarz inequality. Equality holds when recomputation probabilities align with those specified in the theorem. We provide the formal proof of [Theorem 1](#) in [Appendix A](#).

5.2.2 The Top-Query-Edges-Ratio Policy

Based on the analysis, a recomputation policy can calculate the optimal probabilities and recompute the PEs within the top $\gamma\%$ of these probabilities. However, the exact calculation requires the full embeddings of query nodes to obtain the messages ($m_v^{(l)}$) of query nodes, which is infeasible in serving. Thus, instead of computing the full embeddings, we adopt the simplification from prior work [90], whereby our recomputation policy approximates $p_u \propto \frac{|N_Q(u)|}{|N(u)|}$ without considering the message terms. We explain the intuition and highlight the policy’s effectiveness below.

We name our policy *top-query-edges-ratio* since it recomputes PEs with higher ratios of edges from query nodes. For instance, in Fig. 7 (right), the policy recomputes the PEs of nodes 2 and 7. Intuitively, a higher ratio of query edges is likely to change the PE significantly and result in a large approximation error. Empirically, Fig. 6 (right) shows this policy (OMEGA) can recover accuracy drops almost similarly to recomputation based on real approximation errors (AE).

To further assess the effectiveness of OMEGA’s policy, we compare it with two alternatives, IS and RANDOM, as shown in Fig. 6 (right). IS chooses recomputation targets based on node importance scores, defined for each node v as $IS(v) = \frac{1}{\deg(v)} \sum_{u \in N(v)} \frac{1}{\deg(u)}$, following existing sampling-based training methods [19, 20, 90]. Though beneficial for reducing training variance during training, these scores focus more on existing nodes and are less effective for recomputation during serving, resulting in less optimal performance compared to OMEGA’s policy. RANDOM selects targets randomly. This approach fails to identify error-prone PEs, leading to ineffective recovery of accuracy losses, even with large recomputation budgets.

In [Table 3](#), we extensively evaluate OMEGA’s policy across representative GNN models and graph datasets, which shows it can effectively recover accuracy to within 1% point with minimal budget. Our policy consistently outperforms the alternatives, IS and RANDOM, similar to the result in [Fig. 6](#) (right). We extensively evaluate the recomputation policies

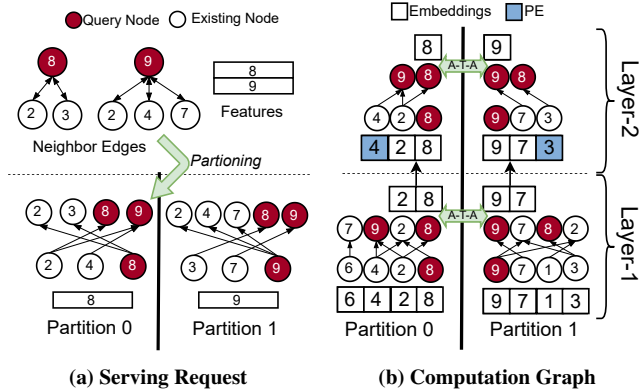


Figure 8: (a) An example serving request on the graph dataset in Fig. 1 with the partitioned requests depicted at the bottom. (b) Partitioned computation graphs for the request.

across various GNN models and graph datasets and observe consistent results in Appendix B.

Finally, OMEGA allows for changing the amount of recomputation through the recomputation budget parameter γ to navigate the tradeoff between accuracy and latency. Users can adjust the parameter depending on the model, dataset, and acceptable percentage of accuracy drop and latency. We evaluate this tradeoff in §8.4 and show that OMEGA can recover accuracy drops with minimal latency increase.

6 Computation Graph Parallelism

While SRPE mitigates the neighborhood explosion problem, communication overhead remains significant. We observe that over 80% of the latency is due to creating computation graphs, which involves fetching feature vectors, PEs, and neighbor edges from remote machines and copying them to GPU memory (§8.3). We now describe *computation graph parallelism* (CGP) to further reduce communication overhead by distributing computation graph creation and execution.

6.1 Distributed Creation and Execution

We describe the key steps in CGP using an example serving request with two batched query nodes (i.e., nodes 8 and 9) at the top of Fig. 8a.

Serving Requests Partitioning. As described in §4, OMEGA’s master first splits incoming serving requests. Specifically, the master evenly assigns partitions to every query node in a request. In our example, nodes 8 and 9 are assigned to partitions 0 and 1, respectively. The edges in a request are then split based on the source nodes’ partitions to enable local aggregation. For instance, the edges whose source nodes are 2, 4, and 8 are included in the partitioned request for partition 0, as depicted at the bottom left of Fig. 8a. The feature vectors of query nodes follow the partitions of the query nodes. The master sends the partitioned edges and features to corresponding computation graph builders.

Computation Graph Generation. Among the edges, each builder uses those having query nodes as destination nodes

to create the last layer of a computation graph (e.g., Layer-2 in Fig. 8b). Each builder then applies OMEGA’s recomputation policy (§5.2.2) to identify recomputation target nodes among the input nodes of the last layer. In Layer-2 of Fig. 8b, while the PEs of nodes 3 and 4 are reused, the embeddings of nodes 2 and 7 are recomputed. For the recomputation, all of the edges terminating at the target nodes need to be included in the other layers. Since the edges are distributed across different partitions, the builders first broadcast their recomputation target nodes to each other through all-gather collective (e.g., nodes 2 and 7), extract the required edges from local graphs (e.g., $4 \rightarrow 2$ and $6 \rightarrow 7$ in Layer-1 of partition 0 in Fig. 8b) and from the partitioned requests (e.g., $8 \rightarrow 2$), then create the remaining layers (e.g., Layer-1 in Fig. 8b).

Layer-wise Distributed Execution. With the computation graphs, GNN executors compute the embeddings of the query nodes by executing GNN layers sequentially. To first compute Layer-1 embeddings, each executor computes partial aggregations using its local features, shuffles them with the other executors through collective communications, and merges them. The output embeddings are concatenated with the local PEs, which are used as the input for the next layer (e.g., Layer-2 input embeddings in Fig. 8). The process is repeated until the query nodes’ embeddings are computed in the last layer execution.

To enable the distributed execution, OMEGA extends conventional message passing (Eq. 1). Instead of applying the aggregation function to the entire neighborhood, OMEGA generates a local aggregation for each partition using the neighbors placed in each partition. OMEGA further defines a merge function to compute global aggregations with the local aggregations. The l -th layer execution is as follows:

$$\begin{aligned}
 a_{v,p}^{(l)} &= \hat{\bigoplus}_{u \in N_p(v)}^{(l)} \{M^{(l)}(h_u^{(l-1)})\}, 0 \leq p < P \\
 h_v^{(l)} &= U^{(l)}(h_v^{(l-1)}, \biguplus_{0 \leq p < P} \{a_{v,p}^{(l)}\})
 \end{aligned} \tag{3}$$

Here, P is the number of partitions, $N_p(v)$ returns the neighbors of a node v in a partition p , $a_{v,p}^{(l)}$ represents a local aggregation for v in p , $\hat{\bigoplus}$ is the local aggregation function, and \biguplus is the merge function. In Fig. 9, we depict the execution of the last layer in our running example.

6.2 Custom Merge Functions

Applying CGP is straightforward for GNN models with commutative and associative aggregations, such as sum or max, but not so for more complex generalized arithmetic aggregations [24, 54] or softmax-based aggregation with learned weights [17, 75]. We explain how to handle them below.

Generalized Arithmetic Aggregation. Beyond simple average functions, some GNN models leverage power mean aggregation [54] or normalized moments aggregation [24]. For power mean aggregation (i.e., $(\frac{1}{|N(v)|} \sum_{u \in N(v)} m_u^p)^{\frac{1}{p}}$), OMEGA computes the local aggregations by summing local messages after applying the $\text{pow}()$ function with p . To merge

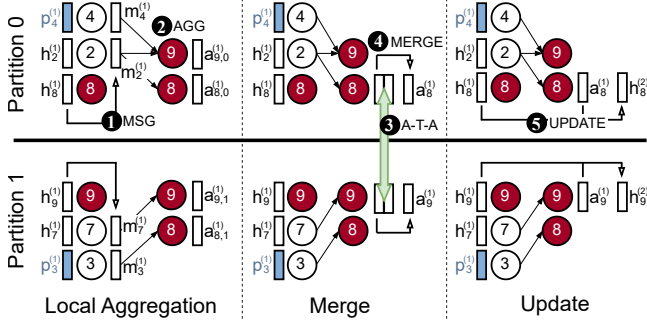


Figure 9: Example of distributed layer execution of CGP. At each partition, **1** the message function is applied to the input embeddings, and **2** the messages are aggregated by the local aggregation functions. **3** The local aggregations of each node are shuffled through all-to-all communications. Then, each partition proceeds to apply **4** the merge function and **5** the update function.

them, OMEGA adds the aggregations and then applies the $\text{pow}()$ function with $1/p$. Normalized moments aggregation (i.e., $(\frac{1}{|N(v)|} \sum_{u \in N(v)} (m_u - \bar{m})^n)^{\frac{1}{n}}$) requires the mean of the messages (\bar{m}). OMEGA first computes the mean values for each destination node (e.g., nodes 8 and 9 in Fig. 9) then broadcasts the values with an all-gather operation. Then, OMEGA computes the global aggregations with the same procedure used in the power mean aggregation.

Softmax-based Aggregation. GNN models can utilize the attention mechanism [17, 75], which learns attention weights using the softmax function [16] to identify important nodes in the neighborhood. To employ the aggregation, a learned attention weight needs to be computed for each edge, which requires the embeddings of destination nodes [75]. For instance, in Fig. 9, the local aggregation in machine 0 for node 9 needs $h_9^{(1)}$, which resides in machine 1. Consequently, OMEGA optionally employs an all-gather operation for destination embeddings (i.e., $h_8^{(1)}$ and $h_9^{(1)}$) to enable local aggregation. Next, the attention weights are normalized using the softmax function. For merging these softmax-based local aggregations while maintaining numerical stability, OMEGA additionally generates the exponential sum of logits and the maximum logits in each partition and adds them to the local aggregations, which are then utilized in the merging step. The two-step aggregation technique for the attention mechanism has recently been applied to Transformer models [26]. We show that the accuracy impact of the aggregation is minimal in §8.2.

We note there are some stateful aggregations [37, 85] to which CGP cannot be directly applied; e.g., those leveraging recurrent neural networks (RNNs) [39] to aggregate messages with recurrent hidden states. The strict dependency on aggregation prevents CGP from computing local aggregations in parallel. Since the RNN model must be sequentially applied to each neighbor in the resulting central aggregation, serving latency can become excessive. For instance, in our measurements of serving latency for a 3-Layer Graph-

Dataset	Nodes	Edges	Avg. Deg.	Features	Hiddens
Reddit [37]	232 K	115 M	492	602	128
Yelp [90]	717 K	14.0 M	20	300	512
Amazon [90]	1.6 M	264 M	168	200	512
Products [43]	2.4 M	124 M	52	100	128
Papers [43]	111 M	1.6 B	14	128	512
FB10B [29]	30 M	10 B	333	1024	128

Table 2: Graph datasets used in the evaluation. The first four columns represent the number of nodes, number of directed edges, average degrees, and feature dimensions. The last column denotes the hidden dimensions used for GNN models.

SAGE [37] model with RNN-based and mean aggregations under identical settings in Table 1, we observe that the RNN-based aggregation requires substantially more time, taking $41 \times$ longer (28.9 s) compared to mean aggregation (702 ms). In future work, we will extend CGP and co-design GNN models to accommodate such aggregations, similar to learnable commutative aggregation [63].

7 Implementation

We implement OMEGA in C++ and Python using the distributed Deep Graph Library (DGL) [78, 96] and PyTorch [64]. OMEGA utilizes DGL’s graph structures and message-passing APIs alongside PyTorch’s DNN operations and communication backends. Communication among computation graph builders relies on PyTorch’s GLOO [9] backend, while the master communicates with other machines using PyTorch RPC [25]. For computation graph execution, OMEGA modifies DGL’s message-passing APIs to substitute global aggregation with local aggregation, all-to-all communication, and merging. It employs DGL for local aggregation, PyTorch’s NCCL [10] for communication, and PyTorch DNN operations for merging. Notably, OMEGA does not require any modification to GNN models written in DGL since OMEGA’s GNN executor is compatible with the APIs of DGL and PyTorch.

8 Evaluation

We evaluate the performance of OMEGA using popular benchmark graph datasets and representative GNN models. We compare DGL-based [78, 96] baseline serving systems with our techniques, SRPE (§5), CGP (§6), and their combination. Our evaluation addresses the following key questions:

- How much does OMEGA improve latency and accuracy compared to the baseline systems (§8.2)?
- To what extent do SRPE and CGP contribute to the reduction in OMEGA’s latency (§8.3)?
- What are the recomputation and memory overheads of using PEs (§8.4)?
- How well does OMEGA scale with additional GPUs and machines (§8.5)?
- How do various system optimizations and model configurations affect OMEGA’s latency (§8.6)?

8.1 Experimental Setup

Testbed. We conducted our experiments on a GPU cluster with 4 servers, each equipped with two 32-core AMD 7542 CPUs, 512 GB of main memory, and two NVIDIA V100S GPUs with 32 GB of memory. The servers are connected with 25 Gbps Ethernet links via a switch. All servers run 64-bit Ubuntu 22.04, DGL v1.0.2, and PyTorch v1.13.0.

GNN Models. We evaluate OMEGA on three representative GNN models, Graph Convolutional Networks (GCN) [52], GraphSAGE (SAGE) [37], and Graph Attention Networks (GAT) [75]. We use two layers for GCN and three layers for SAGE and GAT models to avoid the over-smoothing problem [21, 53, 55] with deeper GNN models.

Datasets. We evaluate OMEGA on six graph datasets detailed in Table 2. Products [43] and Papers [43] are widely used for assessing GNN performance [32, 34, 58, 71]. Reddit [37], Yelp [90], and Amazon [90] represent real-world web services where GNNs power applications like recommendations. For testing OMEGA on a larger scale, we include FB10B, a synthetic dataset with 10 billion edges modeled after Facebook’s social network [29] with randomly generated 1,024-dimensional features, reflecting the high dimensionality in real-world scenarios [42, 89, 92].

Workloads. We synthesize realistic serving workloads from the datasets since no public large-scale GNN serving workload is available. For each dataset, we remove 25% of random test nodes and the edges connected to the nodes. We make a serving request by randomly selecting a specific number of query nodes from the removed nodes and the edges from the query nodes to the nodes in the remaining dataset. Our evaluation uses batch sizes of 64, 128, 256, 512, 1,024, and 2,048. For each batch size, we generate 500 serving requests (reused for all evaluations). We execute one request at a time to measure the serving latency without any resource contention among requests. The reported results are averaged over the 500 serving requests.

Baselines. For a fair comparison with OMEGA, which is based on Distributed DGL (§7), we implement the following two baseline GNN service systems using Distributed DGL [96].¹

- **DGL (FULL)** constructs and executes full computation graphs that consist of the entire k -hop neighborhood of query nodes. This approach is typically preferred for relatively small graphs [41, 91].
- **DGL (NS)** employs neighborhood sampling to reduce latencies at the expense of accuracy. This approach is essential today for supporting large-scale graphs in existing GNN serving systems [56, 72, 89]. We use widely adopted

¹Since DGL is primarily designed for training, we adapt distributed DGL [96] by removing the backward pass and using only the forward pass in both baselines.

Dataset	GCN		SAGE		GAT	
	Acc. (%)	γ (%)	Acc. (%)	γ (%)	Acc. (%)	γ (%)
Reddit	92.5 (-0.1)	0	96.3 (0.0)	0	95.5 (0.0)	0
Yelp	42.4 (-4.5)	20	63.7 (0.0)	0	56.9 (-6.3)	7
Amazon	41.8 (-3.9)	3	79.4 (0.0)	0	63.4 (-3.0)	1
Products	75.6 (+0.1)	0	77.8 (+0.1)	0	73.3 (0.0)	0
Papers	42.0 (+1.4)	0	50.0 (+0.3)	0	49.3 (+0.4)	0

Table 3: Effectiveness of OMEGA’s recomputation policy (§5.2.2). ‘Acc.’ column represents the accuracy with full computation graphs and the percentage of accuracy drops with PEs (without recomputation). ‘ γ ’ column shows the recomputation budget to achieve less than 1% points of accuracy drop. We randomly remove 25% of test nodes to create serving requests, each containing 1,024 query nodes, and compute PEs using the remaining nodes. Accuracy drops and the recomputation budgets are then aggregated across these requests.³

sampling fanouts [37, 49, 72] of (25, 10)² and (15, 10, 5) for models with 2 and 3 layers unless otherwise specified.

Default Configurations. Unless otherwise specified, experiments use a batch size of 1,024 and run on 4 machines, each with 1 GPU. OMEGA employs the recomputation policy (§5.2.2), with budgets (γ) set for less than 1% accuracy drop (Table 3). For the FB10B dataset, containing synthetic feature vectors, no recomputation is performed. Random hash partitioning is applied by default for better load balancing, as locality-aware strategies like Metis [50] do not improve OMEGA or baseline performance (§8.6).

8.2 Overall Performance

We evaluate the end-to-end serving latency and accuracy of OMEGA in comparison to DGL (FULL) and DGL (NS). In Fig. 10, we report the latencies of OMEGA and the baseline systems, along with relative speedups, across six datasets listed in Table 2 and GCN, SAGE, and GAT models. To highlight the contributions of SRPE and CGP, we also include latencies for OMEGA (SRPE) and OMEGA (CGP), representing OMEGA with only SRPE and CGP, respectively.

Compared to DGL (FULL). OMEGA significantly reduces latency while minimizing accuracy drop. For instance, as shown in Fig. 10, OMEGA achieves 159× lower latency than DGL (FULL) for the SAGE model with the Amazon dataset. OMEGA handles large graphs with higher degrees efficiently, leveraging SRPE’s precomputation and CGP’s local aggregation. For the FB10B dataset, OMEGA successfully runs GNNs on the largest dataset by significantly reducing computation graph sizes, whereas DGL (FULL) fails due to CUDA out-of-memory (OOM) errors. The Papers dataset shows little benefit from OMEGA since its serving nodes have low degrees (2.4 on average), and DGL (FULL) shows low latency of 15 ms.

²The (25, 10) fanout means sampling at most 10 neighbors at the first hop and sampling at most 25 neighbors for each direct neighbor.

³We train the models using grid search on learning rates (0.01, 0.001, 0.0001) with the Adam optimizer [51] and dropout probabilities (0.1, 0.5), running fixed numbers of epochs based on convergence. We use neighborhood sampling in training with (25, 10) and (15, 10, 5) fanouts.

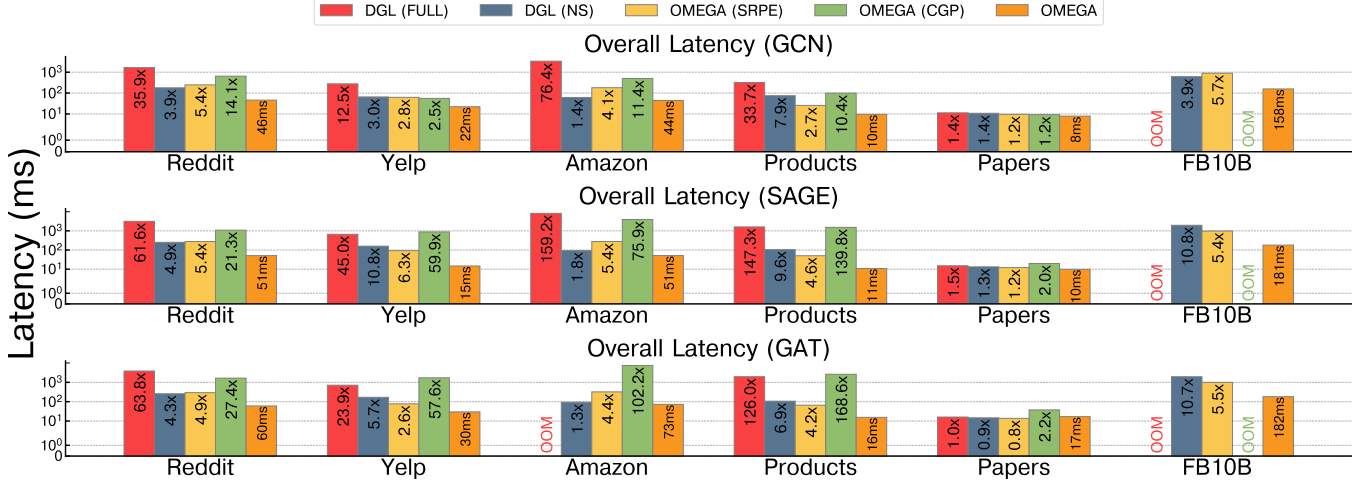


Figure 10: End-to-end serving latency of OMEGA and baseline systems (in log scale) across three models and six datasets. The numbers within each bar represent the latency values for OMEGA or the relative speedup of OMEGA compared to each system. ‘OOM’ indicates that a system failed to execute the workload due to a CUDA Out-of-Memory error.

Systems	Yelp			Amazon		
	GCN	SAGE	GAT	GCN	SAGE	GAT
DGL (NS)	36.2%	63.7%	50.9%	36.1%	79.4%	60.8%
OMEGA	41.5%	63.7%	55.9%	40.9%	79.4%	62.5%

Table 4: Test accuracies of OMEGA and DGL (NS) using three GNN models (GCN, SAGE, GAT) on the Yelp and Amazon datasets. OMEGA employs SRPE with the recomputation budgets from Table 3, maintaining less than 1 % point of accuracy loss. Corresponding latency results are provided in Fig. 10.

Compared to DGL (NS). We first study how neighborhood sampling affects accuracy. For GCN and GAT models on Amazon and Yelp datasets, accuracy loss from sampling compared to OMEGA is significant (1.7% to 5.0% in Table 4), while OMEGA achieves substantial latency speedups (1.3× to 5.7× in Fig. 10) with less than 1% point accuracy loss. SAGE models are more resilient to sampling, typically showing negligible accuracy losses, as reported in prior work [49]. Overall, OMEGA demonstrates minimal accuracy drop while significantly reducing latency across all cases.

Additionally, sampling allows DGL (NS) to handle the largest dataset, FB10B, without CUDA OOM. However, even with sampling, the total neighbors can be large. For instance, with a (15, 10, 5) sampling configuration, one query node can have up to 750 3-hop neighbors, leading to high communication overheads for fetching associated feature vectors, resulting in a latency of 2.0 seconds for FB10B. In contrast, OMEGA effectively reduces computation graph sizes through SRPE and minimizes communication overheads with CGP, outperforming DGL (NS) by up to 10.8×.

8.3 Contributions of OMEGA’s Techniques

To better understand the performance benefits of OMEGA, we analyze the respective improvements from SRPE and CGP.

Contribution of SRPE. We present the latency breakdown and required communication size of DGL (FULL), DGL (NS), OMEGA (SRPE), and OMEGA in Fig. 11. DGL (FULL) suffers from fetching feature vectors and edges for the entire k -hop neighborhood during computation graph creation (Fetch), taking several seconds to serve a single request or causing CUDA OOM. In contrast, SRPE reduces computation graph sizes and communication overhead. For example, in the Amazon dataset, SRPE reduces the communication volume by 18×, from 7.4GB to 411MB, and latency by 29×, from 8.2s to 278ms.

However, compared to DGL (NS), communication size in OMEGA (SRPE) can still be significant, as shown with the Amazon dataset in Fig. 11. This occurs when query nodes have large numbers of direct neighbors (e.g., 168 average degrees in Table 2) and PEs are larger than feature vectors (e.g., 512 hidden vs. 200 feature dimensions for Amazon in Table 2).

Contribution of CGP. CGP’s local aggregation effectively reduces the communication overhead of SRPE, as it only requires collective communications for the query nodes and a small number of recomputation target nodes (e.g., nodes 2, 7, 8, and 9 in Fig. 8b). As shown in Fig. 11 (denoted OMEGA), CGP’s local aggregations effectively minimize communication to a few MBs of necessary collective communications, reducing latency of OMEGA (SRPE) by 5.5× (from 278 ms to 51 ms) and 5.4× (from 978 ms to 181 ms) for the Amazon and FB10B datasets.

On the other hand, We examine CGP’s independent impact using the method in Appendix D. As Fig. 10 shows (denoted OMEGA (CGP)), while CGP reduces latency for 2-hop computation graphs (i.e., GCN) relative to DGL (FULL), its performance for 3-hop graphs (i.e., SAGE, GAT) is poorer since deeper GNN models’ neighborhoods expand to encompass

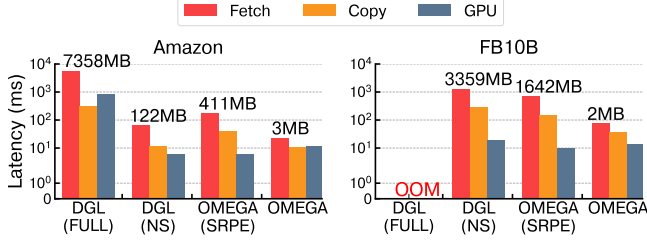


Figure 11: Latency breakdown of SAGE model with Amazon and FB10B datasets in Fig. 10, which consists of three components: ‘Fetch’ builds computation graphs by fetching necessary data (i.e., remote feature vectors, edges, and PEs), ‘Copy’ transfers the data into GPU device memory, and ‘GPU’ runs GNN computations in GPUs (including collective communications for OMEGA’s CGP). The size of data in fetching and collective communications is noted on top of each bar.

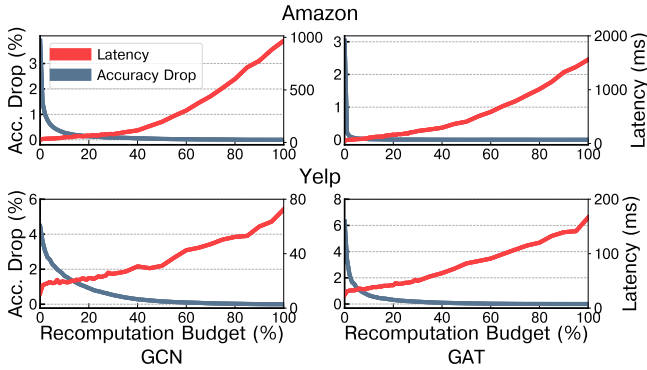


Figure 12: Latency and accuracy trade-off of OMEGA varying recomputation budget with GCN and GAT models and Amazon and Yelp datasets.

most of a dataset, limiting local aggregation effectiveness. Nevertheless, CGP significantly enhances SRPE, where computation graphs mainly consist of first-hop neighbors.

8.4 Recomputation and Memory Overhead of PEs

While SRPE provides significant latency benefits, it also introduces additional costs: recomputation (to mitigate accuracy losses) and memory (to store PEs on the host). We evaluate the impact of recomputation on latency and accuracy, and discuss the memory overhead of PEs.

Recomputation Overhead. We assess the trade-offs between latency and accuracy based on the budget of OMEGA’s recomputation policy (§5.2). Fig. 12 presents results for GCN and GAT models using the Yelp and Amazon datasets, which experience the largest accuracy drops without PE recomputation. *The results demonstrate that OMEGA’s policy effectively minimizes recomputation costs; for instance, a recomputation budget of 7% reduces accuracy losses from 6.3% points to just 1.0% points, while increasing latency by only 11 ms for the GAT model on the Yelp dataset.*

Memory Overhead. The memory required to store PEs is proportional to the number of layers, hidden dimensions, and

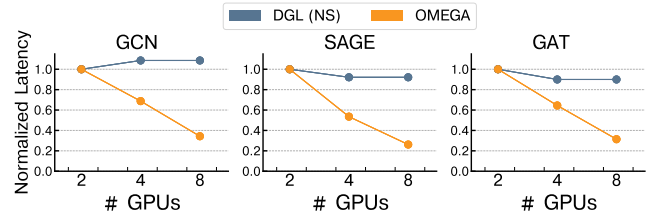


Figure 13: Normalized Latency of OMEGA and DGL (NS) varying number of GPUs with FB10B dataset.

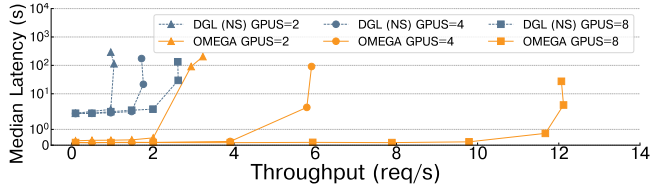


Figure 14: Latency-throughput results of OMEGA and DGL (NS) varying request rates with SAGE model and FB10B dataset.

data type size: $(L - 1) * H * D$ bytes. Although the memory footprint depends on the GNN model configuration and graph dataset size, PEs are typically smaller than the graph dataset size, as models generally have only 2–3 layers and relatively small hidden dimensions [34]. For instance, the memory footprint of PEs for the 3-layer SAGE model is 31.5 GB, representing just 10.9% of the FB10B dataset size.

8.5 Scalability Analysis

In this section, we examine the impact of varying number of machines and GPUs on the latency and throughput of OMEGA. We evaluate the largest FB10B dataset, and compare OMEGA with DGL (NS) since DGL (FULL) cannot run the workload due to CUDA OOM.

Latency. In Fig. 13, we vary the number of GPUs: 2 (on 2 machines), 4 (on 4 machines), and 8 (with 4 machines each using 2 GPUs). While DGL (NS) does not benefit from additional resources due to its centralized execution, OMEGA demonstrates strong scaling by distributing the host-to-GPU memory transfer across multiple GPUs, with each GPU handling only local feature vectors and PEs. *As a result, for instance, the latency of OMEGA with the GAT model decreases by 67% (from 282ms to 88ms), whereas DGL (NS) only shows a 9% (from 2.2s to 2.0s) reduction in latency.*

Throughput. We analyze the throughput of OMEGA and DGL (NS) by modeling request arrivals with a Poisson distribution and feeding workloads into both systems in Fig. 14. While DGL (NS) enables concurrent request handling by individual GPUs, significant network contention limits its scalability, achieving only a 2.6× increase in maximum throughput from 2 to 8 GPUs. In contrast, OMEGA leverages CGP to reduce communication overhead and avoid contention, resulting in a 3.8× increase in throughput. *Furthermore, with 8 GPUs, OMEGA outperforms DGL (NS) by 4.7× while maintaining significantly lower latency.*

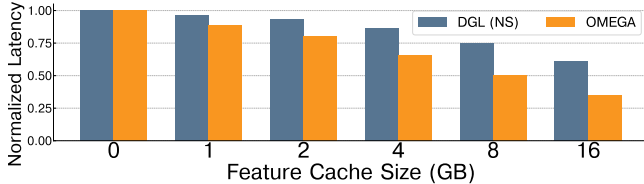


Figure 15: Normalized latency of OMEGA and DGL (NS) varying feature cache size with SAGE model and FB10B dataset.

Systems	Yelp + R.H.	Yelp + Metis	Amazon + R.H.	Amazon + Metis
DGL (FULL)	652.6 ± 30.8	774.2 ± 37.4	8181.3 ± 215.4	10602.8 ± 1087.6
DGL (NS)	159.1 ± 3.2	167.0 ± 8.4	93.0 ± 5.4	100.1 ± 11.4
OMEGA	15.2 ± 0.5	15.3 ± 0.9	49.1 ± 3.3	86.7 ± 11.0

Table 5: Serving latency and standard deviation (in milliseconds) for two graph partitioning strategies (Random-Hash vs. Metis) with Yelp and Amazon datasets.

8.6 Impact of Optimizations and Configurations

We evaluate the impact of system optimizations and model configurations on OMEGA’s latency. To minimize communication and host-to-device transfer overheads, GNN training systems often utilize GPU feature caching [57, 58, 71, 88] and locality-aware partitioning [57, 58, 62, 71, 95, 96]. We analyze these techniques’ effects on OMEGA’s latency and explore various model configurations, including feature dimensions, hidden dimensions, batch sizes, and number of GNN layers.

Impact of Feature Cache. We evaluate how the feature caches in GPUs impact the serving latency of OMEGA and DGL (NS). Following prior work [57], we sort nodes by their out-degrees, caching the highest-ranked nodes to maximize the chances of cache hits. As shown in Fig. 15, both OMEGA and DGL (NS) benefit from caching, but OMEGA sees a much larger reduction in latency. For example, with a 16GB cache, OMEGA’s latency drops by 65%, compared to 39% for DGL (NS). This is because OMEGA takes advantage of CGP’s distributed execution, where each GPU caches frequently accessed nodes from its local subset of data. In contrast, DGL (NS) uses a centralized execution approach, requiring every GPU to consider nodes from the entire dataset.

Impact of Graph Partitioning. We study the impact of graph partitioning on serving latency of OMEGA and the baseline systems using two partitioning strategies: Metis [50], a widely-used locality-aware partitioning method, and random-hash partitioning. As shown in Table 5, we observe that all systems show reduced latency and variance with random hash partitioning compared to using Metis. This suggests that locality-aware partitioning, while effective during the training phase for reducing communication costs, does not provide similar benefits for serving workloads, as query nodes do not fully leverage the locality established before they arrive.

Impact of Model Configurations. In Fig. 16, using the SAGE model on the FB10B dataset, we analyze serving latency across different feature dimensions, hidden dimensions, and batch sizes, where the default values are (1024, 128, 1024).

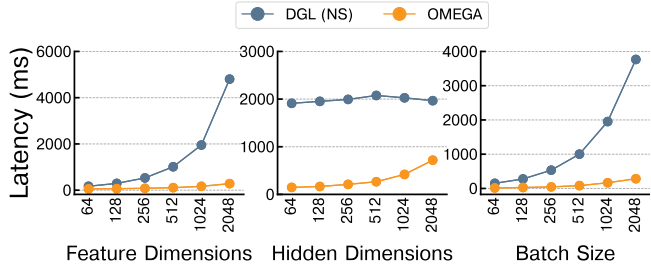


Figure 16: Latency of OMEGA and DGL (NS) varying model hyperparameters and batch sizes with SAGE model and FB10B dataset.

We observe that OMEGA effectively handles larger parameters, outperforming DGL (NS) by 16.9× and 13.3× for feature dimensions and batch size of 2048, respectively. Larger hidden dimensions increase OMEGA’s latency as OMEGA communicates layer embeddings of hidden dimensions (§6.1). Nevertheless, OMEGA achieves 2.7× better latency for 2048 hidden dimensions, leveraging the reduced communication costs by SRPE and CGP. We further evaluate the impact of the number of layers in Appendix C, where we show that OMEGA’s linear latency scaling consistently outperforms baseline systems, particularly for deeper networks.

9 Related Work

GNN Serving Systems. Several systems [56, 72, 89] accelerate GNN serving for large graphs through sampling. However, as discussed in §3.2 and §8.2, sampling often results in significantly higher latency and/or lower accuracy. Other systems [41, 91] focus on resource-efficient techniques for optimizing GNN serving in decentralized environments. While techniques such as adaptive batching [41] can be integrated with OMEGA, serving with the full computation graphs in these systems is prohibitively memory-intensive and slow (§8.2). In contrast, OMEGA effectively reduces serving latency for large graphs while preserving accuracy.

GNN Kernel Optimizations. Existing systems optimize GNN execution on GPUs using techniques like kernel fusion and pipelining to enhance performance [61, 79, 80, 84]. For example, GNNAdvisor [79] reduces atomic operations and global memory access through runtime graph-aware warp and block-level organization. While these optimizations could be integrated into OMEGA, they do not address communication overheads in serving. Similarly, HAG [46] introduces hierarchical aggregation to eliminate redundancy, which is comparable but distinct from CGP’s local aggregation, presenting an interesting future research direction.

GNN Training Systems. Various GNN training systems mitigate overhead from large neighborhoods using approximations, such as sampling or historical embeddings, as discussed in §3.2. Some systems [57, 58, 71, 88] utilize local feature caches to minimize CPU-GPU communication, complementing OMEGA’s approach (§8.6). Full-graph training systems [45, 61, 73, 77], avoid computation graph construction

by operating on the entire graph. However, as they are designed for static graphs and lack dynamic computation graph creation for new query nodes, their techniques are either inapplicable to GNN serving or complementary to OMEGA.

10 Conclusion

This paper presents OMEGA, a GNN serving system achieving low latency and minimal accuracy loss for large graphs. OMEGA addresses neighborhood explosion with SRPE (§5), which precomputes layer embeddings and selectively recomputes error-prone embeddings in the serving phase. OMEGA further reduces communication overhead through CGP (§6), enabling distributed computation graph creation with custom merge functions. Our evaluation demonstrates that OMEGA reduces latency by orders of magnitude compared to baselines with minimal accuracy loss (§8).

References

- [1] NVIDIA A100 Tensor Core GPU. <https://www.nvidia.com/en-us/data-center/a100/>. [Accessed 06-16-2024].
- [2] NVIDIA ConnectX-4 Lx. <https://www.nvidia.com/en-us/networking/ethernet/connectx-4-lx/>. [Accessed 06-16-2024].
- [3] NVIDIA ConnectX-5. <https://www.nvidia.com/en-us/networking/ethernet/connectx-5/>. [Accessed 06-16-2024].
- [4] NVIDIA ConnectX-6 Dx. <https://www.nvidia.com/en-us/networking/ethernet/connectx-6-dx/>. [Accessed 06-16-2024].
- [5] NVIDIA H100 Tensor Core GPU. <https://www.nvidia.com/en-us/data-center/h100/>. [Accessed 06-16-2024].
- [6] NVIDIA Tesla P100. <https://www.nvidia.com/en-us/data-center/tesla-p100/>. [Accessed 06-16-2024].
- [7] NVIDIA V100 Tensor Core GPU. <https://www.nvidia.com/en-us/data-center/v100/>. [Accessed 06-16-2024].
- [8] Build a GNN-based real-time fraud detection solution using Amazon Sagemaker, Amazon Neptune, and the Deep Graph Library. <https://aws.amazon.com/blogs/machine-learning/build-a-gnn-based-real-time-fraud-detection-solution-using-amazon-sagemaker-amazon-neptune-and-the-deep-graph-library/>, 2024. [Accessed 10-09-2024].
- [9] Gloo: a collective communications library. <https://github.com/facebookincubator/gloo>, 2024. [Accessed 10-09-2024].
- [10] NVIDIA NCCL. <https://github.com/NVIDIA/nccl>, 2024. [Accessed 10-09-2024].
- [11] H. Abdine, M. Chatzianastasis, C. Bouyioukos, and M. Vazirgiannis. Prot2text: Multimodal protein’s function generation with gnns and transformers. In *Proceedings of the AAAI Conference on Artificial Intelligence*, volume 38, pages 10757–10765, 2024.
- [12] J. Achiam, S. Adler, S. Agarwal, L. Ahmad, I. Akkaya, F. L. Aleman, D. Almeida, J. Altenschmidt, S. Altman, S. Anadkat, et al. Gpt-4 technical report. *arXiv preprint arXiv:2303.08774*, 2023.
- [13] O. Atkinson, A. Bhardwaj, C. Englert, V. S. Ngairangbam, and M. Spannowsky. Anomaly detection with convolutional graph neural networks. *Journal of High Energy Physics*, 2021(8):1–19, 2021.
- [14] L. Bai, L. Yao, C. Li, X. Wang, and C. Wang. Adaptive graph convolutional recurrent network for traffic forecasting. *Advances in neural information processing systems*, 33:17804–17815, 2020.
- [15] P. Battaglia, J. B. C. Hamrick, V. Bapst, A. Sanchez, V. Zambaldi, M. Malinowski, A. Tacchetti, D. Raposo, A. Santoro, R. Faulkner, C. Gulcehre, F. Song, A. Ballard, J. Gilmer, G. E. Dahl, A. Vaswani, K. Allen, C. Nash, V. J. Langston, C. Dyer, N. Heess, D. Wierstra, P. Kohli, M. Botvinick, O. Vinyals, Y. Li, and R. Pascanu. Relational inductive biases, deep learning, and graph networks. *arXiv*, 2018.
- [16] J. S. Bridle. Probabilistic interpretation of feedforward classification network outputs, with relationships to statistical pattern recognition. In *Neurocomputing: Algorithms, architectures and applications*, pages 227–236. Springer, 1990.
- [17] S. Brody, U. Alon, and E. Yahav. How attentive are graph attention networks? *arXiv preprint arXiv:2105.14491*, 2021.
- [18] T. Brown, B. Mann, N. Ryder, M. Subbiah, J. D. Kaplan, P. Dhariwal, A. Neelakantan, P. Shyam, G. Sastry, A. Askell, S. Agarwal, A. Herbert-Voss, G. Krueger, T. Henighan, R. Child, A. Ramesh, D. Ziegler, J. Wu, C. Winter, C. Hesse, M. Chen, E. Sigler, M. Litwin, S. Gray, B. Chess, J. Clark, C. Berner, S. McCandlish, A. Radford, I. Sutskever, and D. Amodei. Language models are few-shot learners. In H. Larochelle, M. Ranzato, R. Hadsell, M. Balcan, and H. Lin, editors, *Advances in Neural Information Processing Systems*, volume 33, pages 1877–1901. Curran Associates, Inc., 2020.

- [19] J. Chen, T. Ma, and C. Xiao. FastGCN: Fast learning with graph convolutional networks via importance sampling. In *International Conference on Learning Representations*, 2018.
- [20] J. Chen, J. Zhu, and L. Song. Stochastic training of graph convolutional networks with variance reduction. In *International Conference on Machine Learning*, pages 941–949, 2018.
- [21] M. Chen, Z. Wei, Z. Huang, B. Ding, and Y. Li. Simple and deep graph convolutional networks. In *International conference on machine learning*, pages 1725–1735. PMLR, 2020.
- [22] W.-L. Chiang, X. Liu, S. Si, Y. Li, S. Bengio, and C.-J. Hsieh. Cluster-GCN: An efficient algorithm for training deep and large graph convolutional networks. In *Proceedings of the 25th ACM SIGKDD International Conference on Knowledge Discovery & Data Mining, KDD '19*, pages 257–266, New York, NY, USA, 2019. Association for Computing Machinery.
- [23] E. Chien, W.-C. Chang, C.-J. Hsieh, H.-F. Yu, J. Zhang, O. Milenkovic, and I. S. Dhillon. Node feature extraction by self-supervised multi-scale neighborhood prediction. In *International Conference on Learning Representations (ICLR)*, 2022.
- [24] G. Corso, L. Cavalleri, D. Beaini, P. Liò, and P. Veličković. Principal neighbourhood aggregation for graph nets. *Advances in Neural Information Processing Systems*, 33:13260–13271, 2020.
- [25] P. Damania, S. Li, A. Desmaison, A. Azzolini, B. Vaughan, E. Yang, G. Chanan, G. J. Chen, H. Jia, H. Huang, J. Spisak, L. Wehrstedt, L. Hosseini, M. Krishnan, O. Salpekar, P. Belevich, R. Varma, S. Gera, W. Liang, S. Xu, S. Chintala, C. He, A. Ziashahabi, S. Avestimehr, and Z. DeVito. Pytorch RPC: Distributed Deep Learning Built on Tensor-Optimized Remote Procedure Calls. In *Proceedings of Machine Learning and Systems*, 2023.
- [26] T. Dao, D. Fu, S. Ermon, A. Rudra, and C. Ré. FlashAttention: Fast and memory-efficient exact attention with io-awareness. In S. Koyejo, S. Mohamed, A. Agarwal, D. Belgrave, K. Cho, and A. Oh, editors, *Advances in Neural Information Processing Systems*, volume 35, pages 16344–16359. Curran Associates, Inc., 2022.
- [27] S. Deng, H. Rangwala, and Y. Ning. Learning dynamic context graphs for predicting social events. In *Proceedings of the 25th ACM SIGKDD International Conference on Knowledge Discovery & Data Mining, KDD '19*, pages 1007–1016, New York, NY, USA, 2019. Association for Computing Machinery.
- [28] A. Derrow-Pinion, J. She, D. Wong, O. Lange, T. Hester, L. Perez, M. Nunkesser, S. Lee, X. Guo, B. Wiltshire, et al. Eta prediction with graph neural networks in google maps. In *Proceedings of the 30th ACM International Conference on Information & Knowledge Management*, pages 3767–3776, 2021.
- [29] S. Edunov, D. Logothetis, C. Wang, A. Ching, and M. Kabiljo. Generating synthetic social graphs with Darwini. In *2018 IEEE 38th International Conference on Distributed Computing Systems (ICDCS)*, pages 567–577, 2018.
- [30] W. Fan, Y. Ma, Q. Li, Y. He, E. Zhao, J. Tang, and D. Yin. Graph neural networks for social recommendation. In *The World Wide Web Conference, WWW '19*, page 417–426, New York, NY, USA, 2019. Association for Computing Machinery.
- [31] M. Fey and J. E. Lenssen. Fast graph representation learning with PyTorch Geometric. In *ICLR Workshop on Representation Learning on Graphs and Manifolds*, 2019.
- [32] M. Fey, J. E. Lenssen, F. Weichert, and J. Leskovec. GNNAutoScale: Scalable and expressive graph neural networks via historical embeddings. In *International conference on machine learning*, pages 3294–3304. PMLR, 2021.
- [33] A. Fout, J. Byrd, B. Shariat, and A. Ben-Hur. Protein interface prediction using graph convolutional networks. *Advances in neural information processing systems*, 30, 2017.
- [34] S. Gandhi and A. P. Iyer. P3: Distributed deep graph learning at scale. In *15th USENIX Symposium on Operating Systems Design and Implementation (OSDI 21)*, pages 551–568, 2021.
- [35] F. Geyer and S. Bondorf. DeepTMA: Predicting effective contention models for network calculus using graph neural networks. In *IEEE INFOCOM 2019 - IEEE Conference on Computer Communications*, pages 1009–1017, 2019.
- [36] J. Gilmer, S. S. Schoenholz, P. F. Riley, O. Vinyals, and G. E. Dahl. Neural message passing for quantum chemistry. In *International conference on machine learning*, pages 1263–1272. PMLR, 2017.
- [37] W. L. Hamilton, R. Ying, and J. Leskovec. Inductive representation learning on large graphs. In *Proceedings of the 31st International Conference on Neural Information Processing Systems, NIPS'17*, page 1025–1035, Red Hook, NY, USA, 2017. Curran Associates Inc.

- [38] W. L. Hamilton, R. Ying, and J. Leskovec. Representation learning on graphs: Methods and applications. *arXiv preprint arXiv:1709.05584*, 2017.
- [39] S. Hochreiter and J. Schmidhuber. Long short-term memory. *Neural computation*, 9(8):1735–1780, 1997.
- [40] J. Hoffmann, S. Borgeaud, A. Mensch, E. Buchatskaya, T. Cai, E. Rutherford, D. d. L. Casas, L. A. Hendricks, J. Welbl, A. Clark, et al. Training compute-optimal large language models. *arXiv preprint arXiv:2203.15556*, 2022.
- [41] H. Hu, F. Liu, Q. Pei, Y. Yuan, Z. Xu, and L. Wang. λ Grapher: A resource-efficient serverless system for gnn serving through graph sharing. In *The World Wide Web Conference, WWW '24*. Association for Computing Machinery, 2024.
- [42] W. Hu, M. Fey, H. Ren, M. Nakata, Y. Dong, and J. Leskovec. OGB-LSC: A large-scale challenge for machine learning on graphs. In J. Vanschoren and S. Yeung, editors, *Proceedings of the Neural Information Processing Systems Track on Datasets and Benchmarks 1, NeurIPS Datasets and Benchmarks 2021, December 2021, virtual*, 2021.
- [43] W. Hu, M. Fey, M. Zitnik, Y. Dong, H. Ren, B. Liu, M. Catasta, and J. Leskovec. Open Graph Benchmark: Datasets for machine learning on graphs. *Advances in neural information processing systems*, 33:22118–22133, 2020.
- [44] W. Huang, T. Zhang, Y. Rong, and J. Huang. Adaptive sampling towards fast graph representation learning. *Advances in neural information processing systems*, 31, 2018.
- [45] Z. Jia, S. Lin, M. Gao, M. Zaharia, and A. Aiken. Improving the accuracy, scalability, and performance of graph neural networks with ROC. In I. Dhillon, D. Papailiopoulos, and V. Sze, editors, *Proceedings of Machine Learning and Systems*, volume 2, pages 187–198, 2020.
- [46] Z. Jia, S. Lin, R. Ying, J. You, J. Leskovec, and A. Aiken. Redundancy-free computation for graph neural networks. In *Proceedings of the 26th ACM SIGKDD International Conference on Knowledge Discovery & Data Mining, KDD '20*, page 997–1005, New York, NY, USA, 2020. Association for Computing Machinery.
- [47] W. Jiang and J. Luo. Graph neural network for traffic forecasting: A survey. *Expert Systems with Applications*, page 117921, 2022.
- [48] M. Jin, Y. Liu, Y. Zheng, L. Chi, Y.-F. Li, and S. Pan. ANEMONE: graph anomaly detection with multi-scale contrastive learning. In *Proceedings of the 30th ACM International Conference on Information & Knowledge Management*, pages 3122–3126, 2021.
- [49] T. Kaler, N. Stathas, A. Ouyang, A.-S. Iliopoulos, T. Schardl, C. E. Leiserson, and J. Chen. Accelerating training and inference of graph neural networks with fast sampling and pipelining. *Proceedings of Machine Learning and Systems*, 4:172–189, 2022.
- [50] G. Karypis and V. Kumar. A fast and high quality multi-level scheme for partitioning irregular graphs. *SIAM J. Sci. Comput.*, 20(1):359–392, Dec. 1998.
- [51] D. P. Kingma and J. Ba. Adam: A method for stochastic optimization. *arXiv preprint arXiv:1412.6980*, 2014.
- [52] T. N. Kipf and M. Welling. Semi-Supervised Classification with Graph Convolutional Networks. In *Proceedings of the 5th International Conference on Learning Representations, ICLR '17*, 2017.
- [53] G. Li, M. Muller, A. Thabet, and B. Ghanem. DeepGCNs: Can GCNs go as deep as CNNs? In *Proceedings of the IEEE/CVF international conference on computer vision*, pages 9267–9276, 2019.
- [54] G. Li, C. Xiong, A. Thabet, and B. Ghanem. DeeperGCN: All you need to train deeper gcn. *arXiv preprint arXiv:2006.07739*, 2020.
- [55] Q. Li, Z. Han, and X.-M. Wu. Deeper insights into graph convolutional networks for semi-supervised learning. In *Proceedings of the AAAI conference on artificial intelligence*, volume 32, 2018.
- [56] D. Lin, S. Sun, J. Ding, X. Ke, H. Gu, X. Huang, C. Song, X. Zhang, L. Yi, J. Wen, et al. Platogl: Effective and scalable deep graph learning system for graph-enhanced real-time recommendation. In *Proceedings of the 31st ACM International Conference on Information & Knowledge Management*, pages 3302–3311, 2022.
- [57] Z. Lin, C. Li, Y. Miao, Y. Liu, and Y. Xu. PaGraph: Scaling gnn training on large graphs via computation-aware caching. In *Proceedings of the 11th ACM Symposium on Cloud Computing, SoCC '20*, pages 401–415, New York, NY, USA, 2020. Association for Computing Machinery.
- [58] T. Liu, Y. Chen, D. Li, C. Wu, Y. Zhu, J. He, Y. Peng, H. Chen, H. Chen, and C. Guo. BGL: GPU-Efficient GNN training by optimizing graph data I/O and preprocessing. In *20th USENIX Symposium on Networked Systems Design and Implementation (NSDI 23)*, pages 103–118, Boston, MA, Apr. 2023. USENIX Association.

- [59] Y.-C. Lo, S. E. Rensi, W. Torng, and R. B. Altman. Machine learning in chemoinformatics and drug discovery. *Drug Discovery Today*, 23(8):1538 – 1546, 2018.
- [60] M. Lu, Z. Han, S. X. Rao, Z. Zhang, Y. Zhao, Y. Shan, R. Raghunathan, C. Zhang, and J. Jiang. Bright-graph neural networks in real-time fraud detection. In *Proceedings of the 31st ACM International Conference on Information & Knowledge Management*, pages 3342–3351, 2022.
- [61] L. Ma, Z. Yang, Y. Miao, J. Xue, M. Wu, L. Zhou, and Y. Dai. NeuGraph: Parallel deep neural network computation on large graphs. In *2019 USENIX Annual Technical Conference (USENIX ATC 19)*, pages 443–458, Renton, WA, July 2019. USENIX Association.
- [62] V. Md, S. Misra, G. Ma, R. Mohanty, E. Georganas, A. Heinecke, D. Kalamkar, N. K. Ahmed, and S. Avancha. DistGNN: Scalable distributed training for large-scale graph neural networks. In *Proceedings of the International Conference for High Performance Computing, Networking, Storage and Analysis*, pages 1–14, 2021.
- [63] E. Ong and P. Veličković. Learnable commutative monoids for graph neural networks. In *Learning on Graphs Conference*, pages 43–1. PMLR, 2022.
- [64] A. Paszke, S. Gross, S. Chintala, G. Chanan, E. Yang, Z. DeVito, Z. Lin, A. Desmaison, L. Antiga, and A. Lerer. Automatic differentiation in pytorch. 2017.
- [65] J. Peng, Z. Chen, Y. Shao, Y. Shen, L. Chen, and J. Cao. Sancus: staleness-aware communication-avoiding full-graph decentralized training in large-scale graph neural networks. *Proceedings of the VLDB Endowment*, 15(9):1937–1950, 2022.
- [66] J. Shi, V. Chaurasiya, Y. Liu, S. Vij, Y. Wu, S. Kanduri, N. Shah, P. Yu, N. Srivastava, L. Shi, G. Venkataraman, and J. Yu. Embedding based retrieval in friend recommendation. In H. Chen, W. E. Duh, H. Huang, M. P. Kato, J. Mothe, and B. Poblete, editors, *Proceedings of the 46th International ACM SIGIR Conference on Research and Development in Information Retrieval, SIGIR 2023, Taipei*, pages 3330–3334. ACM, 2023.
- [67] Y. Shi, A. Zhang, E. Zhang, Z. Liu, and X. Wang. ReLM: Leveraging language models for enhanced chemical reaction prediction. In *The 2023 Conference on Empirical Methods in Natural Language Processing*, 2023.
- [68] A. Sinha, Z. Shen, Y. Song, H. Ma, D. Eide, B.-J. P. Hsu, and K. Wang. An overview of Microsoft Academic Service (MAS) and applications. In *Proceedings of the 24th International Conference on World Wide Web, WWW '15 Companion*, page 243–246, New York, NY, USA, 2015. Association for Computing Machinery.
- [69] J. M. Stokes, K. Yang, K. Swanson, W. Jin, A. Cubillos-Ruiz, N. M. Donghia, C. R. MacNair, S. French, L. A. Carfrae, Z. Bloom-Ackermann, V. M. Tran, A. Chiappino-Pepe, A. H. Badran, I. W. Andrews, E. J. Chory, G. M. Church, E. D. Brown, T. S. Jaakkola, R. Barzilay, and J. J. Collins. A deep learning approach to antibiotic discovery. *Cell*, 180(4):688 – 702.e13, 2020.
- [70] J. Suarez-Varela, P. Almasan, M. Ferriol-Galmes, K. Rusek, F. Geyer, X. Cheng, X. Shi, S. Xiao, F. Scarselli, A. Cabellos-Aparicio, and P. Barlet-Ros. Graph neural networks for communication networks: Context, use cases and opportunities. *IEEE Network*, pages 1–8, 2022.
- [71] J. Sun, L. Su, Z. Shi, W. Shen, Z. Wang, L. Wang, J. Zhang, Y. Li, W. Yu, J. Zhou, and F. Wu. Legion: Automatically pushing the envelope of Multi-GPU system for Billion-Scale GNN training. In *2023 USENIX Annual Technical Conference (USENIX ATC 23)*, pages 165–179, Boston, MA, July 2023. USENIX Association.
- [72] Z. Tan, X. Yuan, C. He, M.-K. Sit, G. Li, X. Liu, B. Ai, K. Zeng, P. Pietzuch, and L. Mai. Quiver: Supporting GPUs for low-latency, high-throughput GNN serving with workload awareness. *arXiv preprint arXiv:2305.10863*, 2023.
- [73] J. Thorpe, Y. Qiao, J. Eyolfson, S. Teng, G. Hu, Z. Jia, J. Wei, K. Vora, R. Netravali, M. Kim, and G. H. Xu. Dorylus: Affordable, scalable, and accurate GNN training with distributed CPU servers and serverless threads. In *15th USENIX Symposium on Operating Systems Design and Implementation (OSDI 21)*, pages 495–514. USENIX Association, July 2021.
- [74] Y. Tian, H. Song, Z. Wang, H. Wang, Z. Hu, F. Wang, N. V. Chawla, and P. Xu. Graph neural prompting with large language models. In *Proceedings of the AAAI Conference on Artificial Intelligence*, volume 38, pages 19080–19088, 2024.
- [75] P. Veličković, G. Cucurull, A. Casanova, A. Romero, P. Liò, and Y. Bengio. Graph attention networks. In *International Conference on Learning Representations*, 2018.
- [76] S. Virinchi, A. Saladi, and A. Mondal. Recommending related products using graph neural networks in directed graphs. In *Joint European Conference on Machine Learning and Knowledge Discovery in Databases*, pages 541–557. Springer, 2022.

- [77] C. Wan, Y. Li, A. Li, N. S. Kim, and Y. Lin. BNS-GCN: Efficient full-graph training of graph convolutional networks with partition-parallelism and random boundary node sampling. *Proceedings of Machine Learning and Systems*, 4:673–693, 2022.
- [78] M. Wang, D. Zheng, Z. Ye, Q. Gan, M. Li, X. Song, J. Zhou, C. Ma, L. Yu, Y. Gai, T. Xiao, T. He, G. Karypis, J. Li, and Z. Zhang. Deep Graph Library: A graph-centric, highly-performant package for graph neural networks. *arXiv preprint arXiv:1909.01315*, 2019.
- [79] Y. Wang, B. Feng, G. Li, S. Li, L. Deng, Y. Xie, and Y. Ding. GNNAdvisor: An adaptive and efficient runtime system for GNN acceleration on GPUs. In *15th USENIX Symposium on Operating Systems Design and Implementation (OSDI 21)*, pages 515–531. USENIX Association, July 2021.
- [80] Y. Wang, B. Feng, Z. Wang, T. Geng, K. Barker, A. Li, and Y. Ding. MGG: Accelerating graph neural networks with Fine-Grained Intra-Kernel Communication-Computation pipelining on Multi-GPU platforms. In *17th USENIX Symposium on Operating Systems Design and Implementation (OSDI 23)*, pages 779–795, Boston, MA, July 2023. USENIX Association.
- [81] J. Wei, Y. Tay, R. Bommasani, C. Raffel, B. Zoph, S. Borgeaud, D. Yogatama, M. Bosma, D. Zhou, D. Metzler, E. H. Chi, T. Hashimoto, O. Vinyals, P. Liang, J. Dean, and W. Fedus. Emergent abilities of large language models. *Transactions on Machine Learning Research*, 2022.
- [82] Z. Wen and Y. Fang. Augmenting low-resource text classification with graph-grounded pre-training and prompting. In *Proceedings of the 46th International ACM SIGIR Conference on Research and Development in Information Retrieval, SIGIR '23*, page 506–516, New York, NY, USA, 2023. Association for Computing Machinery.
- [83] Y. Wu, D. Lian, Y. Xu, L. Wu, and E. Chen. Graph convolutional networks with markov random field reasoning for social spammer detection. In *Proceedings of the AAAI conference on artificial intelligence*, volume 34, pages 1054–1061, 2020.
- [84] Y. Wu, K. Ma, Z. Cai, T. Jin, B. Li, C. Zheng, J. Cheng, and F. Yu. Seastar: vertex-centric programming for graph neural networks. In *Proceedings of the Sixteenth European Conference on Computer Systems*, pages 359–375, 2021.
- [85] K. Xu, C. Li, Y. Tian, T. Sonobe, K.-i. Kawarabayashi, and S. Jegelka. Representation learning on graphs with jumping knowledge networks. In *International conference on machine learning*, pages 5453–5462. PMLR, 2018.
- [86] H. Yang. AliGraph: A comprehensive graph neural network platform. In *Proceedings of the 25th ACM SIGKDD International Conference on Knowledge Discovery & Data Mining, KDD '19*, pages 3165–3166, New York, NY, USA, 2019. Association for Computing Machinery.
- [87] J. Yang, Z. Liu, S. Xiao, C. Li, D. Lian, S. Agrawal, A. Singh, G. Sun, and X. Xie. GraphFormers: GNN-nested transformers for representation learning on textual graph. In M. Ranzato, A. Beygelzimer, Y. Dauphin, P. Liang, and J. W. Vaughan, editors, *Advances in Neural Information Processing Systems*, volume 34, pages 28798–28810. Curran Associates, Inc., 2021.
- [88] J. Yang, D. Tang, X. Song, L. Wang, Q. Yin, R. Chen, W. Yu, and J. Zhou. GNNLab: a factored system for sample-based gnn training over gpus. In *Proceedings of the Seventeenth European Conference on Computer Systems*, pages 417–434, 2022.
- [89] R. Ying, R. He, K. Chen, P. Eksombatchai, W. L. Hamilton, and J. Leskovec. Graph convolutional neural networks for web-scale recommender systems. In *Proceedings of the 24th ACM SIGKDD International Conference on Knowledge Discovery & Data Mining, KDD '18*, pages 974–983, New York, NY, USA, 2018. Association for Computing Machinery.
- [90] H. Zeng, H. Zhou, A. Srivastava, R. Kannan, and V. K. Prasanna. GraphSAINT: Graph sampling based inductive learning method. In *8th International Conference on Learning Representations, ICLR, Addis Ababa, Ethiopia, April 26-30, 2020*.
- [91] L. Zeng, P. Huang, K. Luo, X. Zhang, Z. Zhou, and X. Chen. Fograph: Enabling real-time deep graph inference with fog computing. In *Proceedings of the ACM Web Conference 2022*, pages 1774–1784, 2022.
- [92] D. Zhang, X. Huang, Z. Liu, J. Zhou, Z. Hu, X. Song, Z. Ge, L. Wang, Z. Zhang, and Y. Qi. AGL: A scalable system for industrial-purpose graph machine learning. *Proc. VLDB Endow.*, 13(12):3125–3137, Aug. 2020.
- [93] S. Zhang, Y. Liu, Y. Sun, and N. Shah. Graph-less neural networks: Teaching old mlps new tricks via distillation. In *The Tenth International Conference on Learning Representations, ICLR, Virtual Event, April 25-29, 2022*.
- [94] X. Zhang, A. Bosselut, M. Yasunaga, H. Ren, P. Liang, C. D. Manning, and J. Leskovec. GreaseLM: Graph REASONing enhanced language models. In *International Conference on Learning Representations*, 2021.

- [95] C. Zheng, H. Chen, Y. Cheng, Z. Song, Y. Wu, C. Li, J. Cheng, H. Yang, and S. Zhang. ByteGNN: efficient graph neural network training at large scale. *Proceedings of the VLDB Endowment*, 15(6):1228–1242, 2022.
- [96] D. Zheng, C. Ma, M. Wang, J. Zhou, Q. Su, X. Song, Q. Gan, Z. Zhang, and G. Karypis. DistDGL: Distributed graph neural network training for billion-scale graphs. In *2020 IEEE/ACM 10th Workshop on Irregular Applications: Architectures and Algorithms (IA3)*, pages 36–44, Los Alamitos, CA, USA, nov 2020. IEEE Computer Society.
- [97] D. Zheng, X. Song, C. Yang, D. LaSalle, and G. Karypis. Distributed hybrid cpu and gpu training for graph neural networks on billion-scale heterogeneous graphs. In *Proceedings of the 28th ACM SIGKDD Conference on Knowledge Discovery and Data Mining*, pages 4582–4591, 2022.
- [98] G. Zhou, X. Zhu, C. Song, Y. Fan, H. Zhu, X. Ma, Y. Yan, J. Jin, H. Li, and K. Gai. Deep interest network for click-through rate prediction. In Y. Guo and F. Farooq, editors, *Proceedings of the 24th ACM SIGKDD International Conference on Knowledge Discovery & Data Mining, KDD, London, UK, August 19-23*, pages 1059–1068. ACM, 2018.
- [99] J. Zhou, G. Cui, S. Hu, Z. Zhang, C. Yang, Z. Liu, L. Wang, C. Li, and M. Sun. Graph neural networks: A review of methods and applications. *AI Open*, 1:57–81, 2020.

A Proof of Theorem 1

We describe the formal proof of [Theorem 1](#). To prove the theorem, we assume each GNN layer independently learns embeddings, following prior works [19, 44, 90]. This assumption allows GNN models to be statistically analyzed despite complex nonlinear activations between layers. Then, as we described in [§5.2.1](#), for each recomputation candidate $u \in R$, we have an unbiased estimator $\hat{f}_u^{(l)} = \frac{1}{p_u} \hat{z}_u q_u^{(l)} + t_u^{(l)}$. Here, $q_u^{(l)} = \sum_{v \in N_Q(u)} \frac{m_v^{(l)}}{|N(u)|}$ and $t_u^{(l)} = \sum_{v \in N_T(u)} \frac{m_v^{(l)}}{|N(u)|}$ where $N_Q(u)$ and $N_T(u)$ represent neighbors of u in query nodes and training nodes, respectively.

Let the embeddings be d -dimensional vectors. We find the optimal recomputation probabilities (p_u), given recomputation budget $\gamma = \sum_{u \in R} p_u$, that minimize the following sum of variances.

$$S = \sum_{i=1}^d \text{Var} \left[\sum_{u \in R} \sum_{l=1}^{k-1} \left(\frac{1}{p_u} \hat{z}_u q_u^{(l)} + t_u^{(l)} \right)_i \right] \quad (4)$$

By the independence of recomputation variables (\hat{z}_u), we have $\text{Cov}[\hat{z}_u, \hat{z}_v] = 0$ if $u \neq v$. Also, $\text{Cov}[\hat{z}_u, \hat{z}_u] = p_u(1 - p_u)$. Thus,

$$\begin{aligned} S &= \sum_{i=1}^d \sum_{u \in R} \left(\sum_{l=1}^{k-1} (q_u^{(l)})_i \right)^2 \frac{1}{p_u^2} p_u(1 - p_u) \\ &= \sum_{u \in R} \sum_{l=1}^{k-1} \left(\sum_{i=1}^d (q_u^{(l)})_i \right)^2 \left(\frac{1}{p_u} - 1 \right) \\ &= \sum_{u \in R} \left\| \sum_{l=1}^{k-1} q_u^{(l)} \right\|^2 \left(\frac{1}{p_u} - 1 \right) \end{aligned} \quad (5)$$

Now, it is sufficient to minimize the first term $\sum_{u \in R} \left\| \sum_{l=1}^{k-1} q_u^{(l)} \right\|^2 \frac{1}{p_u}$. By Cauchy-Schwarz inequality,

$$\left(\sum_{u \in R} \left\| \sum_{l=1}^{k-1} q_u^{(l)} \right\| \frac{1}{\sqrt{p_u}} \right)^2 \left(\sum_{u \in R} \sqrt{p_u} \right)^2 \geq \left(\sum_{u \in R} \left\| \sum_{l=1}^{k-1} q_u^{(l)} \right\| \right)^2 \quad (6)$$

Since $\gamma = \sum_{u \in R} \sqrt{p_u}^2$ and the right-hand side are constants, the first term is minimized when the following equality condition holds:

$$\forall u \in R, \left\| \sum_{l=1}^{k-1} q_u^{(l)} \right\| \frac{1}{\sqrt{p_u}} \propto \sqrt{p_u} \quad (7)$$

Therefore, we conclude S is minimized if $p_u \propto \left\| \sum_{l=1}^{k-1} q_u^{(l)} \right\|^2$.

B Evaluation on Recomputation Policies

In this section, we evaluate the performance of OMEGA’s recomputation policy against RANDOM and IS policies ([§5.2.2](#)). Following the training procedure outlined in [Table 3](#), we train three representative GNN models—GCN, SAGE, and GAT—on six different datasets, as detailed in [Table 6](#). After training, we remove 25% of test nodes (and their connected edges) at random, forming batches of size 1,024. We compute PEs for the training nodes and the remaining 75% of

Dataset	Nodes	Edges	Features	Hiddens	Dropout	GCN (%)	SAGE (%)	GAT (%)
Flickr [90]	89 K	900 K	500	128	0.5	51.8	51.2	51.6
Reddit [37]	232 K	115 M	602	128	0.5	89.3	96.2	95.3
Yelp [90]	717 K	14.0 M	300	512	0.1	42.8	64.0	57.1
Amazon [90]	1.6 M	264 M	200	512	0.1	41.6	79.4	63.4
Products [43]	2.4 M	124 M	100	128	0.5	76.2	78.3	74.1
Papers [43]	111 M	1.6 B	128	512	0.5	47.2	50.9	49.6

Table 6: Datasets used in recomputation policy evaluations. The first three columns describe the number of nodes, edges, and feature dimensions, respectively. The next two columns show the hidden dimensions and dropout probabilities used in training GNN models. Finally, the last three columns show the accuracies of the trained models on each test dataset.

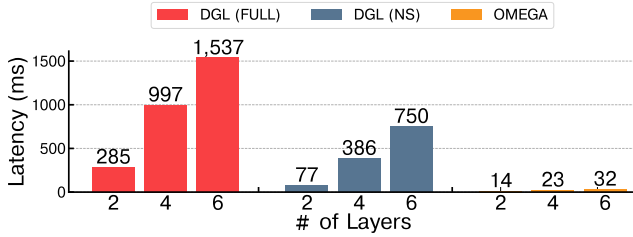


Figure 17: Latency of OMEGA and DGL (NS) varying number of layers with GCNII model and Yelp dataset.

test nodes for each model-dataset pair. We assess the performance of recomputation policies using these batches and PEs and aggregate the results. Fig. 18 shows that OMEGA’s recomputation policy outperforms the baseline policies in most of the cases, effectively narrowing the accuracy gap between full computation graphs and those utilizing SRPE.

C Impact of Number of Layers.

We evaluate the impact of the number of GNN layers on serving latency with GCNII model [21]. As shown in Fig. 17, OMEGA shows a linear increase in latency, while the baselines suffer from an exponential increase. This results in OMEGA outperforming DGL (FULL) and DGL (NS) by $20.3\times$ and $5.5\times$ for 2 layers, and $48.0\times$ and $23.4\times$ for 6 layers, respectively. This is due to PEs allowing OMEGA to construct computation graphs only with direct neighbors, causing the size of the computation graph to grow only linearly with the number of layers. In this evaluation, we use the GCNII model [21], which is designed to support deeper GNN architectures, to mitigate the over-smoothing problem [21, 53, 55], where increasing the number of layers leads to diminishing returns in model accuracy.

D Latency Estimation of CGP

In this section, we describe our estimation of the latency of OMEGA with CGP using execution traces collected in our experiment and the following analytical model. Consider a k -hop computation graph where the i -th layer ($1 \leq i \leq k$) comprises S_i source nodes, D_i destination nodes, and E_i edges. With CGP, each machine sends T bytes of data (including a local aggregation) to each of the remote machines that have desti-

nation nodes (i.e., $T \times \sum_{i=1}^k D_i$ bytes). The amount of host to GPU memory copy is calculated as $(F \times S_1 + E \times \sum_{i=1}^k E_i) / M$ bytes, where F represents the feature dimensions, E is the size of one edge, and M denotes the number of machines. CGP reduces the GPU computation time by a factor of M due to its distributed execution compared to the baseline.

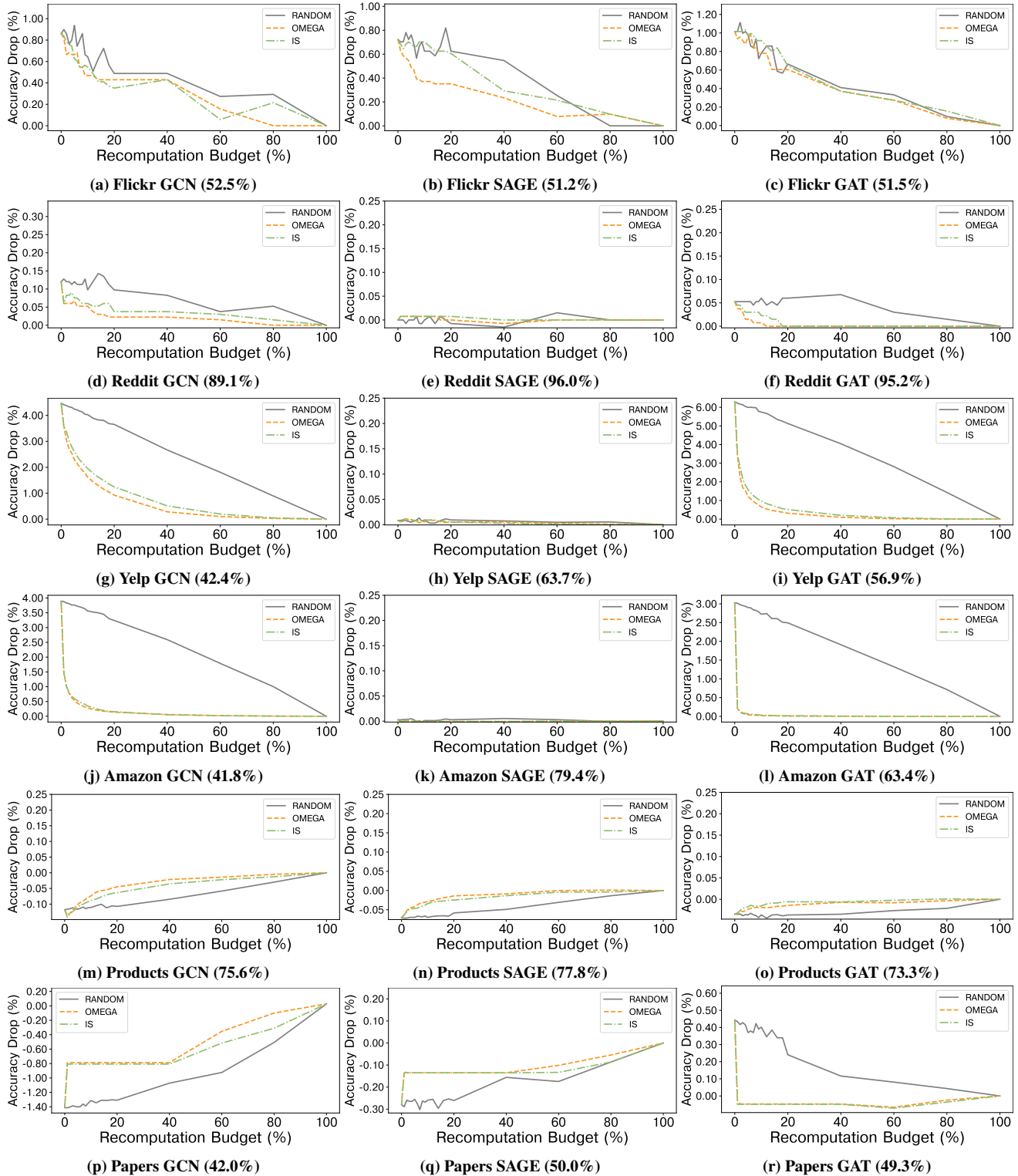


Figure 18: The recovered accuracy varies under different recomputation policies (§5.2.2). Each figure’s caption lists the graph dataset, GNN model, and accuracy with full computation graphs. To evaluate the recomputation policies (i.e., RANDOM, OMEGA, and IS) we randomly remove 25% of test nodes to create batches, each with 1,024 query nodes, and compute PEs using the remaining nodes. Accuracy drops are then aggregated across these batches. We describe the dataset profiles and training settings in Table 3 and Table 6. Note that the model performance reported in Table 6 are measured with the entire test nodes, which can be different the accuracy with full computation graphs here.